PRESSURE CONTROL OF GAS GENERATOR IN THROTTLEABLE DUCTED ROCKETS: A TIME DELAY RESISTANT ADAPTIVE CONTROL APPROACH

A THESIS SUBMITTED TO

THE GRADUATE SCHOOL OF ENGINEERING AND SCIENCE

OF BILKENT UNIVERSITY

IN PARTIAL FULFILLMENT OF THE REQUIREMENTS FOR

THE DEGREE OF

MASTER OF SCIENCE

IN

MECHANICAL ENGINEERING

By

Anıl Alan

June 2017

PRESSURE CONTROL OF GAS GENERATOR IN THROTTLEABLE DUCTED ROCKETS: A TIME DELAY RESISTANT ADAPTIVE CONTROL APPROACH

By Anıl Alan

June 2017

We certify that we have read this thesis and that in our opinion it is fully adequate, in scope and in quality, as a thesis for the degree of Master of Science.

Yıldıray Yıldız(Advisor)

Melih Çakmakçı

Ali Türker Kutay

Approved for the Graduate School of Engineering and Science:

Ezhan Karaşan
Director of the Graduate School

ABSTRACT

PRESSURE CONTROL OF GAS GENERATOR IN THROTTLEABLE DUCTED ROCKETS: A TIME DELAY RESISTANT ADAPTIVE CONTROL APPROACH

Anıl Alan
M.S. in Mechanical Engineering
Advisor: Yıldıray Yıldız
June 2017

Having variable thrust during the operation of a rocket provides tremendous advantages while chasing down a target. For ducted rockets, the key factor to obtain variable thrust is the precise pressure control inside the gas generator, which is one of the main elements of a throttleable ducted rocket and utilized to generate the fuel in gaseous form for combustion. However, the inherent nature of the system makes the control problem difficult due to time varying parameters, nonlinearities and time delays. Furthermore, disturbances and uncertainties exist due to challenging operation conditions. All these challenges make it necessary to design an advanced control approach. Therefore, a delay resistant closed loop reference model adaptive control is proposed in this thesis to address the control problem. The proposed controller combines delay compensation and adaptation with improved transient response. The controller is successfully implemented using an industrial grade cold air test setup, which is a milestone towards obtaining a fully developed throttleable rocket gas generator controller. Simulation and experimental comparisons with alternative adaptive approaches and a fixed controller demonstrate improved performance and effective handling of time delays and uncertainties. A step by step design methodology, covering robustfying schemes, selection of adaptation rates and initial controller parameters, is also provided to facilitate implementations.

Keywords: adaptive control, throttleable ducted rockets, pressure control, gas generator, cold air testing system.

ÖZET

DEĞİŞKEN İTKİLİ KANALLI ROKETLERDE GAZ JENERATÖRÜ BASINÇ KONTROLÜ: ZAMAN GECİKMESİNE DİRENÇLİ ADAPTİF KONTROL YAKLAŞIMI

Anıl Alan
Makine Mühendisliği, Yüksek Lisans
Tez Danışmanı: Yıldıray Yıldız
Haziran 2017

Operasyon sırasında itki değişimi yapabilen roketler, hareketli bir hedefi takip ederken büyük bir avantaja sahiptirler. Kanallı roketler için bu avantajı sağlamanın anahtarı, temel alt elemanlarından birisi olan gaz jeneratörü içerisinde yüksek hassasiyetle basınç kontrolü yapmaktır. Ancak, sistemin doğası bu kontrol problemini zorlaştırmaktadır, çünkü, sistemin modeli zaman değişimlidir ve doğrusal değildir. Dahası, zorlu çalışma koşullarından dolayı sistemde bilinmezlik ve dış bozucu etkenler gözlemlenmektedir. Açık literatürde bu kontrol problemine getirilen çözümler genel olarak doğrusal kontrolcü yaklaşımlarını içermektedir. Ancak problemin zorluğu, literatürde yer alan çalışmalardan farklı bir yaklaşıma ihtiyaç olduğunu göstermektedir. Bu nedenle, bu tezde, bir "zaman gecikmesine dirençli kapalı döngü referans modelli adaptif kontrolcü" geliştirilerek kontrol probleminin daha etkili bir şekilde çözümü sağlanmıştır. Önerilen kontrolcü, zaman gecikmesi direnci ve düzeltilmiş geçici tepki iyileştirmelerini bünyesinde barındırır. Kontrolcü, değişken itkili kanallı roket çalışmalarında bir kilometre taşı olarak kullanılan soğuk hava akış test sistemine başarılı bir şekilde gömülmüştür. Nümerik simülasyon ve testler sonucunda, önerilen kontrolcünün, farklı adaptif kontrolcülere ve sabit kazançlı bir kontrolcüye kıyasla daha yüksek bir zaman gecikmesi direnci ile iyileştirilmiş bir performans ortaya koyduğu gözlemlenmiştir. Adaptif kontrolcüler için adım adım tasarım prosedürü, gürbüzlüğü artırıcı metot, adaptasyon oranı ve başlangıç durumları belirleme konuları da kontrolcü tasarımını kolaylaştırmak adına tezde ele alınmıştır.

Anahtar sözcükler: adaptif kontrol, değişken itkili kanallı roket, basınç kontrolü, gaz jeneratörü, soğuk hava akış test sistemi.

Acknowledgement

First of all, I want to express my sincere gratitude to my valuable advisor Yıldıray Yıldız for his generous support and unlimited guidance throughout my graduate study. He not only improved my knowledge and vision in control studies, but also enlightened my path in academic and personal life.

I want to thank to my thesis committee, Melih Çakmakçı and Ali Türker Kutay for their time and valuable suggestions. I also thank to my friends in lab group, Negin Musavi, Shahab Tohidi and Ehsan Yousefi for our discussions and conversations. A well deserved acknowledgment also goes to Ümit Poyraz with whom we spent a lot of time around the experimental setup and faced challenges, failures and finally success together.

This study has been an unexpectedly long journey with a lot of uncertainties for me and I can't thank to all my friends enough for making it bearable. Starting with my dearest cousin Candeniz Alan, Ali Gökdemir, Ozan Güler, Doğukan Gür, Burak Çeşnigil and Yusuf Önalan have been in my life forever. I want to acknowledge Arda Akay, Mesut Bostancı, Can Baloğlu, Talha Köse, Utku Göreke, Mehmetcan Karabulut, Çağatay Doğan, Burak Diker, Bahadır Yılmazer, Emre Yılmaz, Seçil Kocatepe, Ezgi Altıntaş, Sercan Bayram, Atakan Arı, Çağatay Karakan, Mehmet Kelleci and Selçuk Erbil for their comfort and friendship.

I wish to thank to my parents, Erdoğan Alan and Gülay Alan, for all the opportunities they provided me by hard work and sacrifice. Nothing would be possible without them on my back. I thank to Özün for being the greatest sister ever and her unlimited patience.

Last but not least, I want to thank to Funda because having her in my life eases my burden and makes me a better person.

Contents

List of Figures

List of Tables

Chapter 1

Introduction

1.1 Objective of the Study

Smart ammunition is becoming more relevant with the advance of the technology. Guided missiles are now hunted down by other air defense missiles during operation. In order to operate successfully, missiles should be technologically superior compared to their counterparts. One of the technological advantages is the ability to alter speed during operation. By doing so, rockets can sustain optimum performance for different flight conditions. Besides, they can slow down while turning and go faster in a straight path, which makes their maneuvers more efficient. This ability, which is called as throttleability, is very important for air defense missiles and it increases the missile's no-escape zone, which is the maximum range that the missile can outrun its target [3].

In order to achieve the throttleability, one needs to understand the underlying dynamics yielding propulsion. Missiles produce thrust as an outcome of chemical reactions of a propellant with an oxidizer, which is called a burning process. Propulsion systems can be divided into two groups when it comes to finding the source of the oxidizer that is required for the combustion. Air breathing jet engines provide the oxidizer from the surrounding atmosphere, whereas non-air

breathing jet engines carry their oxidizer along with the fuel, which makes them a closed system. Conventional solid rocket engines are examples to non-air breathing jet engines. They are relatively easy to manufacture, since they don't contain complex parts, and produce a fixed thrust performance over a variety of flight conditions thanks to their closed system property. In addition to their advantage of simplicity, their thrust can be controlled (Variable Thrust Solid Propulsion Systems [4]). However, their specific impulse, which is the total impulse that the rocket engine can produce per unit propellant burnt, are very low compared to air breathing engine systems since they have to carry their oxidizers as well, which makes them less preferable for long range cruise flights. Air breathing jet engines, on the other hand, take the air from the atmosphere during an operation, compress it to different levels using various methods (ramjets, scramjets, turbojets, turbofans etc.) and mix it with the fuel to have the combustion and yield thrust.

Ramjet is a type of air breathing jet engine, which utilizes the forward motion of the missile to collect and compress air with the air-intake openings. Ramjets can be categorized into two groups according to their fuel types, solid fuel (SFRJ) and liquid fuel ramjets (LFRJ). Liquid fuel is injected to combustion chamber to meet with the compressed air in LFRJ. Thrust level of the engine is determined by the flow rate of the injected fuel, which yields throttleability. However, injection of the fuel in LFRJs requires complex and expensive systems. Also, air breathing engines suffer from flameout problem, which is the die out of the flame in the combustion chamber. LFRJ, as a member of air-breathing engine, needs a flame stabilizer in order to avoid this problem, which increases the complexity of the design. SFRJ, on the other hand, is simple in general. Solid Fuel Integrated Ramjets (SFIRJ) is an example to SFRJ, which contains solid fuel on the outer shell of the rocket engine with a hole in center to enable compressed air flow through. Ablation is the fuel injection process for these systems, which makes it very hard to control the injected fuel flow rate. Therefore, SFIRJs are not preferred for the cases where a good amount of throttleability is required. Ducted rockets, however, are tailored for this purpose and can be classified as an SFRJ with a specific fuel injection methodology to allowing better control over fuel flow

rate.

1.1.1 Throttleable Ducted Rockets

Ducted rockets (DR), like ramjet engines, utilize the forward motion of the rocket to 'inhale' the air from surroundings and compress it using air-intake nozzles. Air is then proceeded to the ram combuster (RC). There is a gas generator (GG) element whose duty is to provide the oxidizer deficient fuel in appropriate form to RC, where the main combustion process occurs by a mixture of the air from the air-intakes and the fuel from GG (see Fig. 1.1).

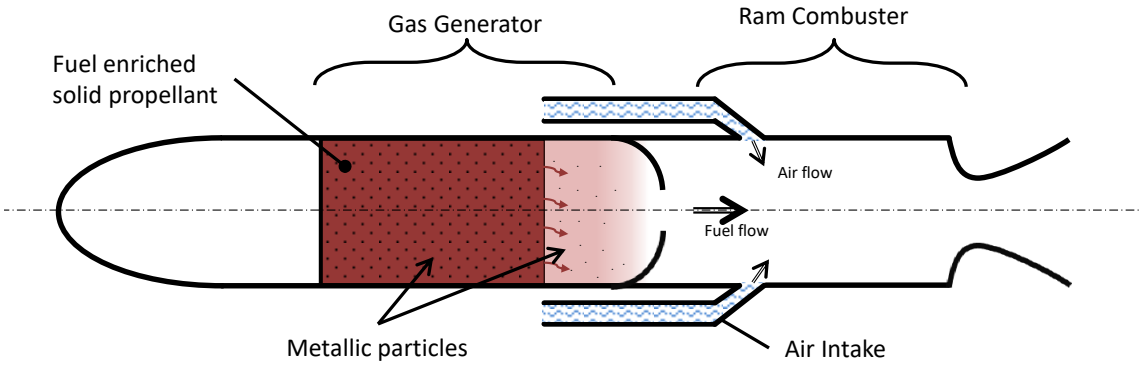

Figure 1.1: Ducted rocket components

In the GG, fuel is formed by a pre-burn process from the solid propellant and sent through a connection between GG and RC by means of the pressure difference. What is appealing about DR is the possibility to control the fuel injection supplied by GG. Throttleable Ducted Rockets (TDR), also known as Variable Flow Ducted Rockets, use various methods to have variable fuel flow rate injected to combustion chamber in a controlled manner. These systems combine the advantages of different propulsion systems: higher specific impulse values of air breathing engines, simplicity of the solid rocket engines and throttleability of the LFRJs. They also don't need a flame stabilizer for the flameout problem, because the hot gas from the GG is able to maintain combustion [5]. Although the specific impulse value in TDR is high, some metallic particles (boron or

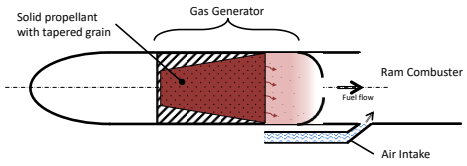

(a) Changing the burning area of the propellant

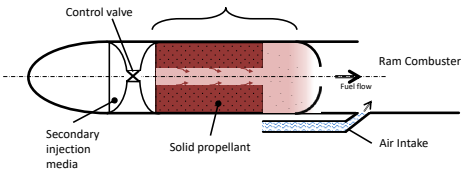

(b) Using secondary injection

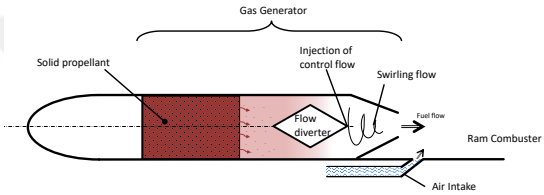

(c) Using a vortex valve

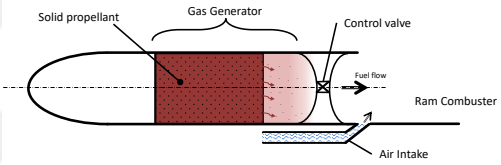

(d) Using a control valve

Figure 1.2: Methods of regulating the fuel flow rate from GG to RC (figures originated from [1] and [2]).

aluminum) are placed inside the solid propellant to enhance it further [6, 7]. These particles are not burnt at initial burning process at GG and carried to RC with the fuel.

1.1.2 Variable Thrust in Throttleable Ducted Rockets

Fuel flow rate generated by the GG is one of the main concerns in TDR since it directly affects the thrust of the rocket. Having a variable fuel flow rate from the GG to the RC can be realized using several different methods listed below [1, 2]:

- Changing the burning area of the propellant in the GG in a controlled manner (see Fig. 1.2a): Assuming the solid propellant burns with uniform cross sectional area (so-called cigarette type burning), their solid grains can be trimmed to have different cross sectional areas at each moment of burn. A smaller burning area generates less fuel, then yields less thrust. However, this method is available only before ignition. Once a trimmed propellant is

ignited, it is unlikely to make changes on its geometric structure. Therefore, solid rocket engines with trimmed propellants have prescribed thrust profile over the whole operation region.

- Introducing secondary injection to the GG chamber to control the burning rate (see Fig. 1.2b): It is known that the burning rate of a solid propellant is affected by the pressure of the chamber [8]. This property is called as the pressure sensitivity of the propellant. Burning rate of the solid propellant can be controlled by means of controlling the pressure at the GG chamber by introducing a secondary medium. However, it requires complex parts such as a secondary chamber and a control valve, which contradicts the advantage of TDR being simple compared to LFRJ engines.

- Utilizing a vortex valve which introduces a swirl to the flow in order to control the effective throat area (see Fig. 1.2c): Injected fuel flow rate from the GG to the RC can be shown to directly depend on the effective throat area between the two elements. Therefore, changing the effective throat area can be counted as a way of manipulating the fuel flow rate. A vortex valve can inject a swirling flow at the throat to increase the flow resistance (or reduce the effective throat area) at the expense of increasing the system complexity.

- Changing the throat area between the GG and the RC using a control valve (see Fig. 1.2d): Effective throat area between the GG and the RC can be varied using a control valve, which is less complex than the vortex valve.

Among these methods of regulating the fuel mass flow rate, changing the throat area using a control valve is the most commonly used approach [1, 9, 10, 11, 12]. Miller et al. [1] proposed placing mechanical elements into the throat between the GG and the RC, and they studied the effects of the different inserting positions and the geometries of the structures on the flow rate. Using a decision matrix for design, they found out that side inserted plug is the best mechanical element for this purpose (See. Fig. 1.3a and 1.3b). A piston-like structure is inserted in the throat from the side in this solution. Niu et al. [13], on the other hand, favored

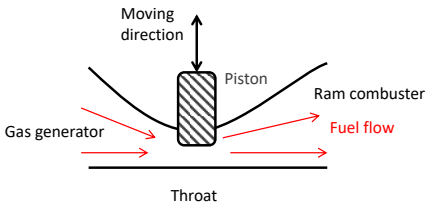

(a) Throat area regulation with piston, front view

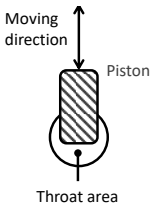

(b) Throat area regulation with piston, side view

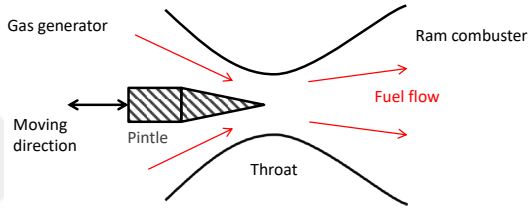

(c) Throat area regulation with pintle

Figure 1.3: Different mechanical elements for throat area regulation (figures originated from [1]).

the needle-type (or pintle-type) valve (see Fig. 1.3c) by mentioning its simplicity and high sensitivity which is defined as the effect of one unit of movement on the resultant throat area change. One disadvantage of the pintle-type structure is that its geometry is more prone to degeneration due to high operating temperatures and metallic particles flowing with the fuel.

Actuation method is also another issue to be considered for throat area regulation. Some studies [14, 13, 9] favors the pressure-balanced gas regulating systems as the actuator, whereas others [7, 15, 16] deem the electromechanical actuation more suitable for changing the throat area.

1.2 Motivation of the Study

In order for ducted rockets to have aforementioned advantages over their counterparts during a flight mission, their speed needs to be controlled continuously. The main motivation for throttleability is to have control over the speed of ducted

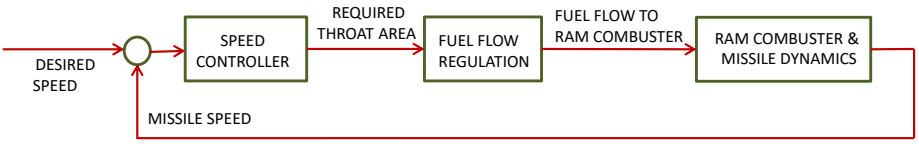

(a) First alternative of the speed control loop

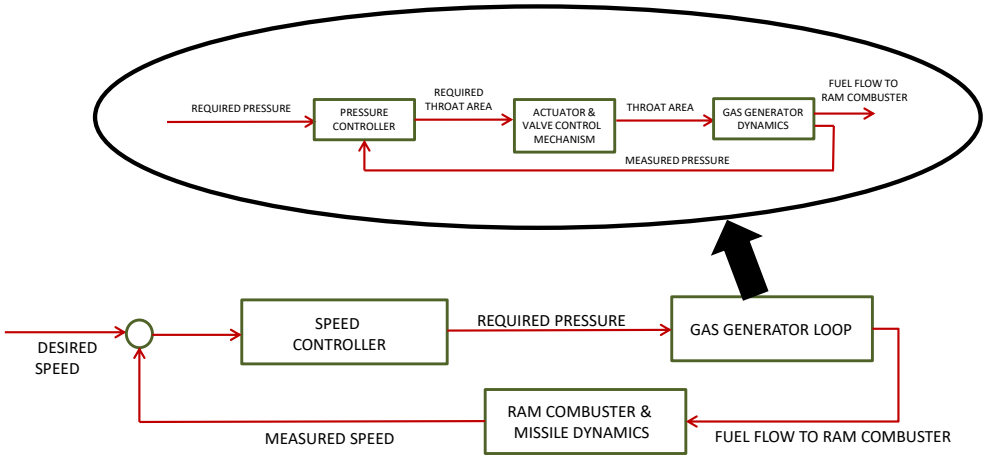

(b) Second alternative of the speed control loop

Figure 1.4: Alternative speed control loops of a TDR.

rockets by changing their thrust, which is possible via fuel flow rate regulation. There are two alternatives for the speed control loop structure of a throttleable ducted rocket. Firstly, pressure inside the gas generator (GG) can be directly controlled by the speed controller. In this case, the loop is formed with a speed controller, fuel flow regulation, ram combuster (RC) and missile dynamics (see Fig. 1.4a). Speed controller calculates the necessary throat area between the GG and the RC to minimize the difference between the desired and the actual missile speeds. Bao et al. [9, 10, 11, 14, 12], in their successive studies, design thrust control loops using this method in order to have precise control over the speed of the ducted rocket.

Second alternative methodology for the speed control of TDR is to implement an inner pressure control loop. In this case, the speed control loop has a hierarchical structure where an outer loop is driven by the error between the desired and the actual speed and determines the required GG pressure to minimize this

error. Required GG pressure is then provided to the inner feedback loop as a reference, which controls the mass fuel flow rate to achieve the desired pressure (see Fig. 1.4b) [3, 17, 18, 19].

The motivation of the second method having pressure control loop arises from the gas pressure stability. Although the first method appears to be simpler, it doesn't contain an explicit structure to keep the gas pressure inside GG within safe levels, which may cause pressure build up and structural damage in case of a disturbance. In the second method, on the other hand, required fuel mass flow rate is provided along with keeping the gas pressure stable thanks to the gas pressure controller. The GG pressure control loop in the second method is the focus of this thesis.

1.2.1 Literature Search and Contribution of This Study

Existing studies, regarding the control problem of the gas generator (GG) pressure, mainly involves linearization of nonlinear dynamics around equilibrium points and designing controllers based on these points. Linear feedback controllers are the most common approach in the literature. Sreenatha et al. [18] use a linear proportional-integral (PI) controller as the pressure controller of the throttleable ducted rocket (TDR). They show that the PI controller is able to control the system with sufficient tracking performance in simulations. However, no experimental results are provided. Niu et al. [13] also design a PI controller based on linear matrix inequality method and provide experimental results.

Other than nonlinear dynamics, another challenge for the controller design is that the free volume inside the GG increases with time, which makes the system time varying. Pinto et al [19], Joner et at. [20] and Bergmans et al. [16] address this problem by introducing gain scheduling methods to their linear controllers. They tailor their controller gains according to the free volume inside the GG and provide successful implementation results. Another method, which is employed for the flight performance evaluation study of the Meteor missile, is called 'the performance funnel' [7, 21]. In this approach, a proportional controller is utilized

with a time varying gain, which is adjusted online to keep the error of the closed loop system within a predefined performance funnel.

Gas generators are not unique to throttleable ducted rocket systems. They are also utilized in other types of air breathing engines, such as air turbo rocket. In their work [15], Ostrander and Thomas study GG pressure dynamics for an air turbo rocket. They conduct experiments in an open loop fashion for modeling purposes. In another study of the same authors [22], they develop a nonlinear mathematical model and match the simulations of that model with the open loop experimental results. Closed loop controller design is left as future study. Peterson et al. [23] work on the GG pressure control for a hybrid rocket engine, where they assign a linear proportional-integral-derivative (PID) controller as the pressure controller. Gains of the controller are chosen by trial-and-error using simulations. They obtain reasonable experimental results in a cold air test setup (CATS). However, the performance of the proposed controller in [23] against a disturbance, which is the nozzle erosion, lacks necessary robustness.

In Variable Thrust Solid Propulsion Systems (VTSPS), burning of the solid propellant is the main combustion process to yield thrust. Thereby, fuel gas is not discharged to any other element (no ram combuster). The gas pressure is controlled using similar strategies as are used for the GG of TDR. Davis and Gerards worked on the pressure control problem of VTSPS [24], where they appoint a linear PI controller in the pressure control loop and tune the gains via trial-and-error.

In this study, we propose an alternative method to address the GG pressure control problem, which contains nonlinear dynamics and time varying parameters, by eliminating the need for a precise system model for gain scheduling, which is the common approach in the open literature. This is achieved by utilizing an adaptive controller, which includes a unique combination of the elements of the Adaptive Posicast Controller (APC) studied by Yildiz et al. in [25] and closed loop reference model (CRM) adaptive controller proposed in [26, 27, 28]. The newly proposed controller structure is named as delay resistant closed-loop reference model (DR-CRM) adaptive control. In the following two subsections,

the components of the proposed controller, APC and CRM, are explained.

1.2.1.a Adaptive Posicast Control

Adaptive posicast control (APC) is an adaptive controller developed for time delay systems which extends the ideas from the Smith Predictor [29], finite spectrum assignment [30] and adaptation [31, 32, 33]. The ability of the APC to accommodate large delays has been successfully validated through several simulation and experimental studies presented in [34, 35, 36, 37, 38, 39]. Other notable studies on the adaptive control of time delay systems can be seen in [40], where unknown input delays and [41], where both state and input delays are addressed. Also, extension of predictor feedback to nonlinear and delay adaptive systems with actuator dynamics modeled by partial differential equations can be found in [42].

1.2.1.b Closed-loop Reference Model Adaptive Control

A well-known trade off in model reference adaptive control (MRAC) is that if the adaptation rate, which is a free design parameter to determine the speed of the adaptation in adaptive systems, is increased, fast convergence of the closed loop system to the reference model, which serves as a model for the closed loop dynamics to follow, is provided at the cost of high frequency oscillations. Recently, a new class of adaptive control system has been proposed to address this issue: Closed loop reference model (CRM) adaptive control, proposed in [26, 27, 43, 28, 44], introduces an error feedback modification to the reference model, which is shown to improve the transient response. Similar approaches where the reference model is modified to obtain better transients can be found in [45, 46, 47, 48].

1.3 Cold Air Testing System

In throttleable ducted rocket (TDR) research, cold air test setup (CATS) is widely appointed as the crucial step in validation of subsystems and methods. In CATS

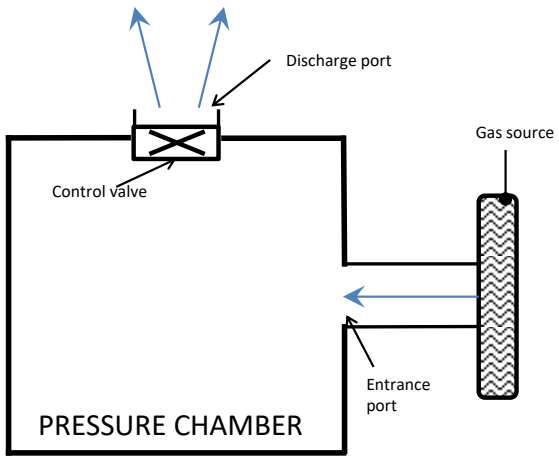

Figure 1.5: Simple representation of cold air test setup

(see Fig. 1.5), there is a pressure chamber with two ports, one entrance and one discharge. Entrance port is connected to a gas supply that provides a continuous mass flow rate of gas to the chamber. Discharge port has a control valve to manipulate the throat area in order to control the gas pressure inside the chamber. CATS imitates the gas generator (GG) based on the working principle: Burning of the solid propellant supplies a continuous mass flow rate of fuel and the control valve at the throat between the GG and the RC is utilized to control the gas pressure inside the GG. However, other than parametric variations arising from different gas temperatures, there are two main differences between these two systems. Firstly, the pressure chamber has constant volume in CATS, whereas it increases with time in the GG because the gas fills the volume once occupied by the solid propellant but emptied due to burning. Secondly, the inlet mass flow rate of the fuel in the GG is a function of the pressure due to the pressure sensitivity of the solid propellant. However, in CATS, there is no direct connection between the pressure in the chamber and flow rate of the gas. Still, the advantage of CATS providing cheap and simple experiments are used in the industry in order to gain insight and experience in TDR subsystems. CATS is used, for

example, to validate the numerical simulation results of flow characteristics, to test the structures in control valve that is used to change the throat area and to characterize the materials that are planned to be used in the construction [49, 50, 51, 52, 53, 54]. Employed pressure controller of the GG in TDR is also an important subsystem that is required to be qualified and CATS has been utilized to conduct comparative analysis of alternative control systems [23], which is then used to acquire a proper control methodology based on the gained insight. In this study, using the facilities provided by Roketsan Inc., an industrial grade CATS is constructed and employed to validate the proposed controller and compare it by various competing methods.

1.4 Organization of the Thesis

Chapter 1 includes the introduction to the thesis. Main control problem is explained along with the different approaches that are utilized in the literature. Motivation of this study is described by providing the state of the art in the field and the gaps that need to be filled.

Chapter 2 contains the mathematical modeling of both the gas generator (GG) and the cold air testing system (CATS). Several throat area modulation mechanisms are introduced and analyzed geometrically, and full nonlinear models are obtained. In order to facilitate the controller design, models are simplified.

The controller approaches selected for the controller problem are presented in Chapter 3. Sequential controller improvement steps are explained, starting from MRAC and ending with the DR-CRM adaptive control. A constant gain proportional-integral controller is also designed to reveal the performance improvements provided by the adaptive controllers. Implementation enhancements of adaptive controllers along with a simple step-by-step controller design procedure is added. Finally, simulation results are given considering both the GG and CATS, employing full nonlinear system models.

Chapter 4 introduces the experimental cold air testing setup in detail. Then, comparative experimental results with the designed controllers implemented on the test setup are shown.

Chapter 5 concludes this thesis with a general summary and discusses possible directions for future studies.

Chapter 2

System Model

Control efforts generally require information about the plant that is planned to be controlled. Therefore, the usual initial step in control studies is to get the mathematical model of the plant which contains governing differential equations. Mathematical modeling is crucial not only for the controller design, but also for numerical simulations. It is simpler and easier to run several simulations compared to conducting a single experiment. Therefore, simulations are widely employed to validate and improve the controller performance before the experimental phase.

In this chapter, the mathematical model of the gas pressure dynamics inside the gas generator of a throttleable ducted rocket is derived. In the modeling process, all the elements in the system are considered. These elements are shown in Fig. 2.1 and listed as

- Gas generator (GG).
- Actuator, which is a closed loop system consisting of a driver card, a brushless direct current motor operated in position mode and an encoder.
- Valve dynamics, which consists of the valve equation and drive-train elements.

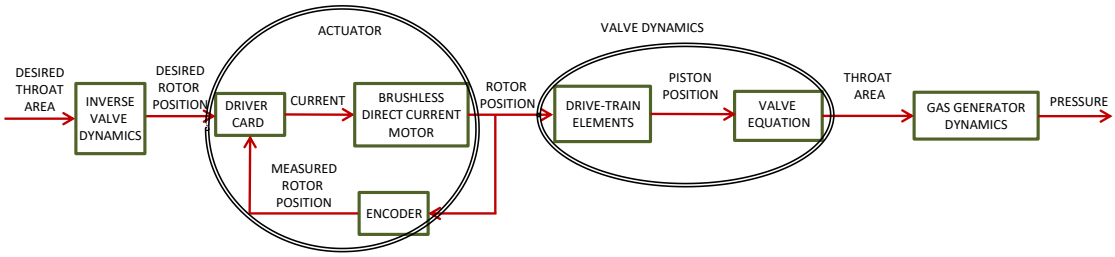

Figure 2.1: Elements in the gas generator system

The output of the model, which is the pressure inside the GG, is controlled by changing the throat area between the GG and the ram combuster (RC). Control objective is to determine the desired throat area for the pressure chamber to have the desired pressure dictated by the outer loop speed controller (see Fig. 1.4b). Pressure controller output, which is the desired throat area, is realized through the actuator and valve dynamics after being converted to the desired rotor position of the actuator by using the inverse of the valve dynamics. The actuator is a closed loop system with its driver card driving the brushless direct current motor by the error between the desired and the measured values of the actuator rotor. The encoder measures the rotor position. Drive-train elements are used to convert the rotational motion of the actuator to translational motion of the throat-changing-element, which is chosen as the piston for gas generator, with required amount of reduction. The movement of the piston alters the throat area between the gas generator and the ram combuster. (see Fig. 1.3a and 1.3b).

Similar elements exist in the cold air testing setup (CATS) model, the block diagram of which is shown in Fig. 2.2. One major difference is in the selection of throat-changing-element, which is a conical pintle in CATS (see Fig. 1.3c). The reason for this selection is that CATS has milder experimental conditions compared to the GG due to the temperature difference and absence of metallic particles. Therefore, it is possible to use a throat-changing-element which yields a higher amount of sensitivity, which is defined as the effect of linear movement of the element on the resultant throat area change, in CATS without any concern in degradation of the element that is inevitable in the GG experiments. After obtaining the mathematical model of the system, some modeling enhancements are applied using experimental data in order to improve the fidelity of the model

for simulations.

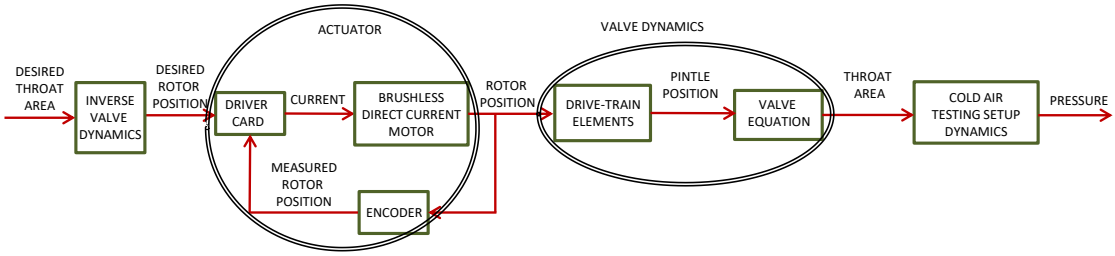

Figure 2.2: Elements in the cold air testing system

2.1 Throttleable Ducted Rocket Gas Generator

2.1.1 Gas Generator Dynamics

In the case of gas generator (GG) pressure control, model of the plant is the mathematical relationship described by a nonlinear time varying differential equation between the throat area (input) and the GG pressure (output). This relationship is studied by many groups [17, 55, 6, 19, 9, 7, 3]. The modeling steps shown here are concurrent with the literature.

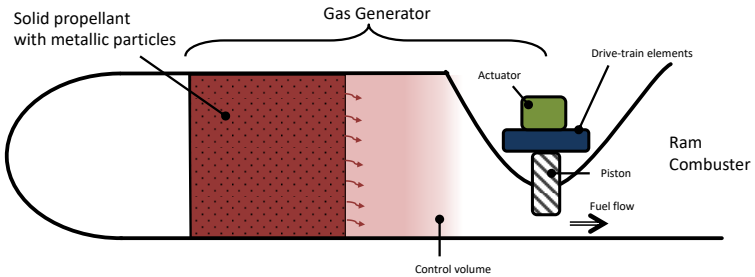

Figure 2.3: Schematic of the gas generator control volume

Consider the GG section in Fig. 2.3. With the assumption of uniform cross sectional area burning (cigarette type burning) for the propellant, the mass flow rate into the control volume is given as

$$\dot{m}_b = A_b r \rho \tag{2.1}$$

where $\dot{m}_b$ [kg/sec] is the mass flow rate of the burnt propellant and A_b [m^2], r [m/s] and ρ [kg/m^3] are uniform burning cross sectional area, burning rate and density of the solid propellant, respectively. The conventional power law for the burning rate r is given as ([56])

$$r = aP_g{}^n \tag{2.2}$$

where a is the empirical constant dependent on the temperature of the GG and n is the pressure sensitivity of the propellant [8]. Both of the constants are found empirically for the type of propellant used and specific burning conditions. P_g [Pa] is the GG pressure. Defining $c_1 \equiv A_b a \rho$ and combining (2.1) and (2.2), it is obtained that

$$\dot{m}_b = c_1 P_g^n. \tag{2.3}$$

Mass flow coming out of the control volume is a function of the throat area between the GG and the ram combuster (A_t [m^2]) and the pressure inside the control volume (P_g). Assuming chocked flow conditions at the throat, the relationship between the throat area and the resulting mass flow rate out of the control volume, $\dot{m}_{out}$ [kg/sec] is given by [17]

$$\dot{m}_{out} = A_t \frac{P_g}{\sqrt{T}} \sqrt{\frac{\gamma}{R}} (\frac{\gamma+1}{2})^{-\frac{\gamma+1}{2\gamma-2}} = \frac{P_g A_t}{c^*} \tag{2.4}$$

where γ is the specific heat ratio, c^* [m/s] is the characteristic velocity of the gas inside the control volume, T [K] is the GG temperature and R [J/(kg K)] is the specific gas constant.

Assuming ideal gas conditions for the fuel in the control volume, ideal gas equation is given as,

$$P_g V_g = m_g R T \tag{2.5}$$

where V_g [m^3] is the volume of the control volume and m_g [kg] is the mass of the gas inside the control volume. It is further assumed that the process inside the control volume is isothermal (i.e. $\dot{T} = 0$). It is noted that V_g is a function of time because as the solid propellant burns, its volume is filled with gas. By taking these into consideration, the time derivative of the ideal gas law (2.5) is found using the chain rule, given as

$$\dot{P}_g V_g + P_g \dot{V}_g = \dot{m}_g R T = (\dot{m}_b - \dot{m}_{out}) R T. \tag{2.6}$$

Using (2.3) and (2.4), (2.6) can be rewritten as

$$\dot{P}_g = P_g^n \frac{c_1 RT}{V_g} - P_g \frac{A_t RT}{V_g c^*} - P_g \frac{\dot{V}_g}{V_g}. \tag{2.7}$$

It is noted that the rate of change of V_g can be found using the burning rate,

$$\dot{V}_g = A_b r = A_b a P_g^n.$$

Defining $c_2 \equiv A_b a$,

$$\dot{V}_g = c_2 P_g^n. \tag{2.8}$$

Putting (2.8) into (2.7), it is obtained that

$$\dot{P}_g = P_g^n \frac{c_1 RT}{V_g} - P_g \frac{A_t RT}{V_g c^*} - P_g^{n+1} \frac{c_2}{V_g}.$$

By defining constants $c_3 \equiv c_1 RT$ and $c_4 \equiv \frac{RT}{c^*}$, the time varying and nonlinear differential equation for the GG pressure can be reached as

$$\dot{P}_g = P_g^n \frac{c_3}{V_g} - P_g \frac{A_t c_4}{V_g} - P_g^{n+1} \frac{c_2}{V_g}. \tag{2.9}$$

2.1.2 Actuator

A brushless DC motor is used in position controller mode as the actuator, with its driver card and an encoder to measure the position/speed of the rotor. The closed loop actuator dynamics is approximated as a first order linear system. Furthermore, experiments revealed that a considerable amount of time delay exists in the communication between the actuator driver and the software where the controller algorithms will be embedded in. Therefore, the actuator transfer function is given as

$$W_{act}(s) = \frac{\theta(t)}{\theta_{com}(t)} = \frac{e^{-\tau s}}{\tau_{act} s + 1} \tag{2.10}$$

where θ [quadrature] is the realized rotational position of the rotor while θ_{com} [quadrature] is commanded rotational position (4000 quadratures (qc) correspond to 1 rotation), τ_{act} [sec] is actuator closed loop time constant and τ [sec] is the time delay.

2.1.3 Valve Geometry and Drive-Train Elements

The drive-train elements consist of a gear box and a spindle to convert the rotational motion of the motor into the translational motion of a piston at the throat area. The linear position of the piston determines the throat opening. Below, the detailed valve and the drive train models are provided.

2.1.3.a Valve Geometry in Piston Element Case

The throat opening between the gas generator and the ram combuster is projected on a 2D surface as a circle (see Fig. 2.4). The linear motion of the piston (depicted as a rectangle in the 2D drawings) changes the open throat area. There

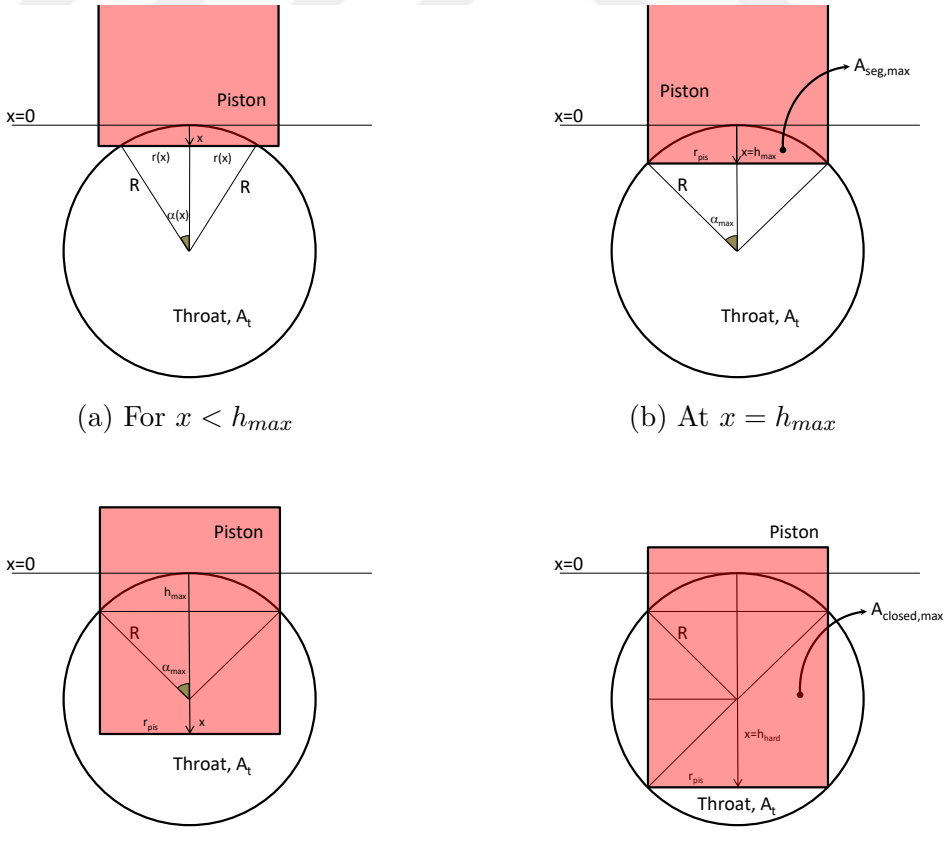

(a) For $x < h_{max}$

(b) At $x = h_{max}$

(c) For $h_{hard} > x > h_{max}$

(d) At $x = h_{hard}$

Figure 2.4: Analytical approach to the throat area problem for piston-in-throat case.

exists a nontrival relationship between the movement of the piston and the minimum throat area, where the choked flow conditions occur, due to their complex geometries. In this study, however, the size of the open throat area is approximated as the projection of the real area in order to simplify the modeling. The shaded area within the circle in Fig. 2.4 represents the closed area by the piston, whereas the unshaded area inside the circle is regarded as the open throat area.

Further analysis of the geometric modeling problem shows that there are two phases in calculating the shaded area. In the first phase, the linear position of the piston is smaller than or equal to a critical value, called as h_{max}, which indicates that only a portion of the piston shades a segment in the circle (Fig. 2.4a). In the second phase, after the critical position is passed, motion of the piston shades the circle directly proportional to its displacement (Fig. 2.4c). There is also a hard limit on the piston movement that indicates the maximum shaded area, which represents the minimum open throat area (Fig. 2.4d). A hard limit on the minimum throat area is desired since it protects the system from rapid pressure build up in case of a malfunction in the closed loop system. The detailed geometric analysis of both phases are shown below.

- **Up to h_{max} (Fig. 2.4a):** The shaded segment in the circle grows as the linear motion of the piston is increased for this phase. The length of the chord $2r(x)$ [m], which is the line that links two points on a circle, in this case is a function of the piston position x [m]. It is found geometrically as,

$$r(x) = \sqrt{R^2 - (R - x)^2} \tag{2.11}$$

  where R [m] is the radius of the fully open throat area. The angle $\alpha(x)$ [deg] can be found using basic trigonometric relationship

$$\alpha(x) = \sin^{-1}\left(\frac{r(x)}{R}\right). \tag{2.12}$$

  The shaded segment, A_{cl} [m^2], is then given as

$$A_{cl}(x) = R^2\left(\frac{\pi 2\alpha(x)}{360} - \frac{\sin(2\alpha(x))}{2}\right) \tag{2.13}$$

  where $\alpha(x)$ is in degrees.

- **After h_{max} (Fig. 2.4c):** The shaded segment in the circle reaches its maximum in this case ($A_{seg,max}$, see Fig. 2.4b). The chord r becomes equal to the radius of the piston r_{pis} [m], the angle α reaches to its maximum value, α_{max} [deg], which is given as

$$\alpha_{max} = \sin^{-1}\left(\frac{r_{pis}}{R}\right). \tag{2.14}$$

The critical point, h_{max} [m], is then calculated as

$$h_{max} = R - \frac{r_{pis}}{\tan(\alpha_{max})} \tag{2.15}$$

The shaded area in this case increases proportionally with the motion of the piston and calculated as

$$A_{cl}(x) = A_{seg,max} + 2r_{pis}(x - h_{max}) \tag{2.16}$$

where $A_{seg,max}$ [m^2] is given as

$$A_{seg,max} = R^2\left(\frac{\pi 2\alpha_{max}}{360} - \frac{\sin(2\alpha_{max})}{2}\right) \tag{2.17}$$

where α_{max} is in degrees. The hard limit on the piston position, h_{hard} [m], can be found as

$$h_{hard} = h_{max} + 2\sqrt{R^2 - r_{pis}^2}. \tag{2.18}$$

In overall, the relationship between the linear position of the piston and the shaded area in the circle is calculated as,

$$A_{cl}(x) = \begin{cases} R^2\left(\frac{\pi 2\alpha(x)}{360} - \frac{\sin(2\alpha(x))}{2}\right) & \text{if } \ 0 \le x \le h_{max} \\ R^2\left(\frac{\pi 2\alpha_{max}}{360} - \frac{\sin(2\alpha_{max})}{2}\right) + 2r_{pis}(x - h_{max}) & \text{if } \ h_{max} < x \le h_{hard}. \end{cases} \tag{2.19}$$

The open throat area, A_t [m^2] for all cases is found as

$$A_t(x) = \pi R^2 - A_{cl}(x). \tag{2.20}$$

Graphical representation of the throat area with respect to the linear position of the piston is given in Fig. 2.5 for a fully open throat radius $R = 15$ mm

and piston radius $r_{pis} = 12$ mm. It can be concluded from the graph that the relationship is linear for most of the operation region. Another possible design criteria is considered in Fig. 2.6 where piston radius is chosen as the design parameter and its effect on the minimum throat area is studied. It is noted that fully open throat radius is selected as $R = 15$ mm for this case. Minimum throat area directly affects the maximum gas generator pressure and it can be observed that the piston radius should be selected around 12 mm for this case to reach the highest pressure values.

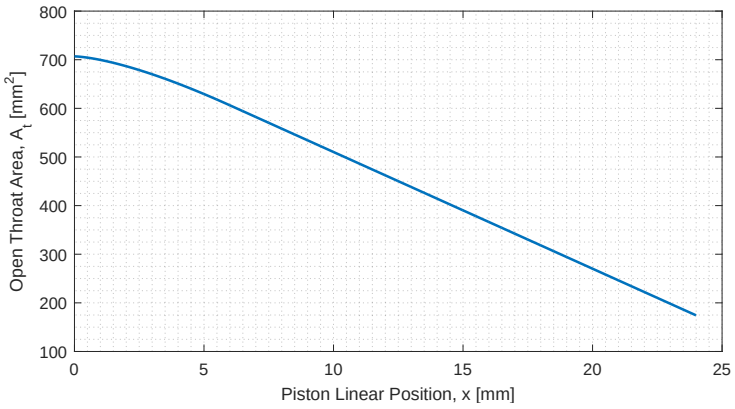

Figure 2.5: Linear position of the piston vs. corresponding open throat area for $R = 15$ mm and $r_{pis} = 12mm$.

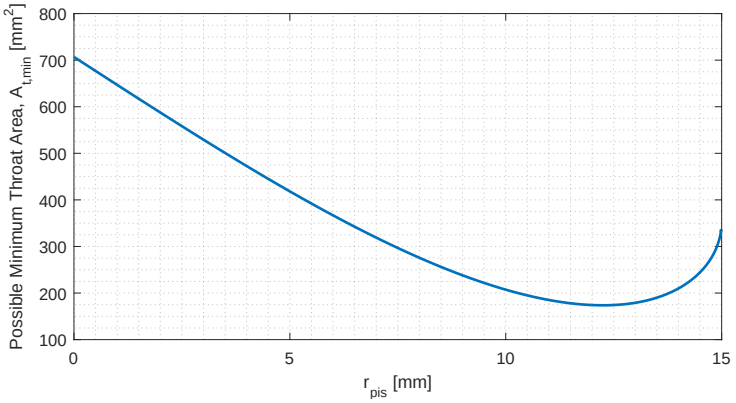

Figure 2.6: The effect of the piston radius on minimum achievable throat area for $R = 15$ mm.

2.1.3.b Drive-Train Elements

A gear box with a reduction ratio of $1 : R_1$ is used to increase the torque output of the actuator. The spindle has an R_2 [m] thread pitch, i.e. one turn of rotation corresponds to R_2 [m] translational motion. Therefore, the relationship between the actuator rotational position, θ [quadrature], and the linear position of the piston, x [m], can be calculated as

$$x = \frac{\theta R_2}{4000 R_1} \tag{2.21}$$

where 4000 quadratures (qc) correspond to 1 rotation.

2.1.4 Modeling for Controller Design

To facilitate the controller design, a simpler model is developed following the steps listed below:

- Nonlinear plant model and valve equation in (2.9) and (2.20), respectively, are linearized.
- Actuator dynamics are ignored due to small time constants compared to the plant.
- Inverse valve dynamics is employed in series with the controller.

Equation (2.9) provides the mathematical relationship, in a compact way, between the variable that is desired to be controlled, which is the GG pressure P_g and the control input, which is the throat area A_t. It is noted that this relationship is not only nonlinear but also time-varying, due to the changing control volume V_g inside the GG. It is known that nonlinearity and time-varying dynamics make the controller design a challenging task. One approach can be linearizing the system dynamics around an equilibrium point by assuming a constant V_g. This procedure is explained below.

Making the following definitions

$$c_5 \equiv \frac{c_3}{V_{g0}}$$
$$c_6 \equiv \frac{c_4}{V_{g0}}$$
$$c_7 \equiv \frac{c_2}{V_{g0}}$$

for a constant volume V_{g0}, (2.9) can be rewritten as

$$\dot{P}_g = c_5 P_g^n - c_6 P_g A_t - c_7 P_g^{n+1} \tag{2.22}$$

Linearizing around an equilibrium GG pressure, P_{g0}, and the corresponding throat area, A_{t0}, by using Taylor linearization method, which is given as

$$f(x,u) \approx f(x_0,u_0) + \left.\frac{\partial f}{\partial x}\right|_{\substack{x=x_0\\u=u_0}} (x-x_0) + \left.\frac{\partial f}{\partial u}\right|_{\substack{x=x_0\\u=u_0}} (u-u_0) + \cancel{h.o.t.} \tag{2.23}$$

for $f(x,u) = \dot{P}_g$ where $x = P_g$, $u = A_t$, $x_0 = P_{g0}$ and $u_0 = A_{t0}$, it is obtained that

$$\dot{P}_g = \Delta\dot{P}_g = c_8 \Delta P_g + c_9 \Delta A_t \tag{2.24}$$

where $\Delta P_g = P_g - P_{g0}$ and $\Delta A_t = A_t - A_{t0}$ and

$$c_8 \equiv n P_{g0}^{n-1} c_5 - A_{t0} c_6 - (n+1) P_{g0}^n c_7$$
$$c_9 \equiv -P_{g0} c_6.$$

When the actuator time constant τ_{act}, (2.10), is obtained using open loop experiments, it is revealed that it can be neglected compared to gas generator pressure dynamics due to being much faster. Therefore, we ignore the first order actuator dynamics for controller design, but keep the time delay, τ, into consideration, which yields an equation of

$$\frac{\theta(t)}{\theta_{com}(t)} = e^{-\tau s}. \tag{2.25}$$

The relationship between the position of the piston (input) and the throat area (output) in valve equation (2.20) is observed to be linear at $x > h_{max}$, which dominates the overall operation regime since $h_{max} \ll h_{hard}$ for reasonable geometric

values of R and r_{pis} (see Fig. 2.5). Therefore, we neglect the nonlinearity at $x < h_{max}$ and assume that valve equation is linear in terms of input and output:

$$A_t = c_{10} + c_{11}x \tag{2.26}$$

where

$$c_{10} \equiv R^2\left(\pi - \frac{\pi 2\alpha_{max}}{360} + \frac{\sin(2\alpha_{max})}{2}\right) + 2r_{pis}h_{max}$$
$$c_{11} \equiv -2r_{pis}.$$

It is also noted that the relationship between the actuator rotational position, θ, and the position of the piston, x, is linear in (2.21). Therefore if (2.21) is put in (2.26), the valve dynamics for controller design can obtained as

$$A_t = c_{10} + c_{12}\theta \tag{2.27}$$

where

$$c_{12} \equiv c_{11}\frac{R_2}{4000R_1}$$

and θ is in units of quadratures and A_t is in m^2.

It is noted that the inverse of valve dynamics (2.27) is used to convert the required throat area determined by the pressure controller to the required actuator rotational position, which is provided to the actuator as a reference (see Fig. 2.1). By doing this so, we can cancel out valve dynamics. In overall, together with the actuator time lag, τ, the system model used to develop the controller is obtained as

$$W_p(s) = \frac{\Delta P(t)}{\Delta A_{t,com}(t)} = \frac{c_9 e^{-s\tau}}{s - c_8} \tag{2.28}$$

where $A_{t,com}$ is the commanded throat area, calculated by the pressure controller. Model for controller design is shown in Fig. 2.7.

2.2 Cold Air Testing Setup

Overall cold air test setup (CATS) consists of a control volume (pressure chamber), an actuator, a valve mechanism, drive-train elements, a gas supply and

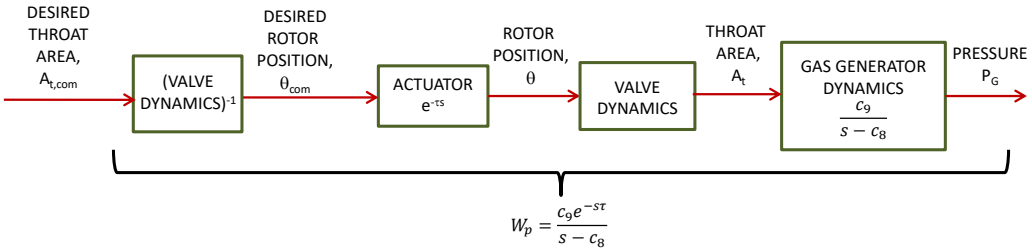

Figure 2.7: Model for controller design

a pressure regulator (see Fig. 2.8). A continuous flow of gas is provided by a nitrogen source to the plant from the inlet and flow is adjusted by a pressure regulator. The output of the model, which is the pressure inside the control volume, is controlled through changing the exit throat area of the flow, which is the model input. The throat area is increased/decreased using the linear motion of a pintle at the exit throat. Drive-train elements are used to convert the rotational motion of the actuator, which is a brushless direct current motor, to translational motion of the pintle with required amount of reduction.

2.2.1 Plant

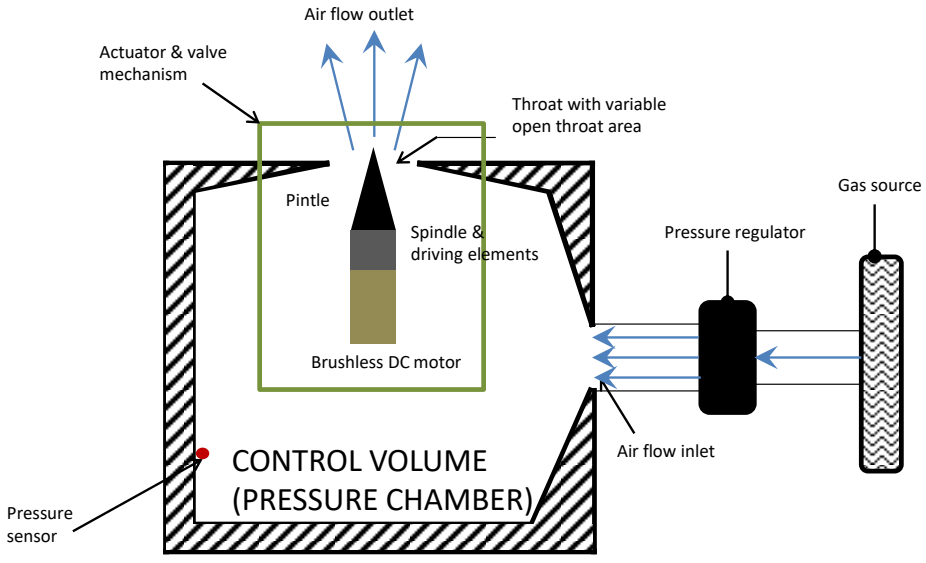

Figure 2.8: Schematic of cold air test setup

Assuming ideal gas conditions, the difference between the mass flow rates going into the control volume (pressure chamber), $\dot{m}_{in}$ [kg/sec], and going out of the control volume, $\dot{m}_{out}$ [kg/sec], is given as

$$\dot{m}_{in} - \dot{m}_{out} = \frac{\dot{P}V}{RT} \tag{2.29}$$

where R [J/(kg K)] is the specific gas constant and P [Pa], T [K] and V [m^3] are the pressure, the temperature and the volume of the gas inside the control volume. The process is assumed to be isothermal with no change in the control volume, hence $\dot{V} = \dot{T} = 0$.

Mass flow coming out of the control volume is a function of the throat area (A_t [m^2]) and the pressure inside the control volume (P). Assuming chocked flow conditions, the relationship between the throat area and the resulting mass flow rate out of the control volume is given by [17]

$$\dot{m}_{out} = PA_t((\frac{2}{\gamma+1})^{(\frac{\gamma}{\gamma-1})})\sqrt{\frac{\gamma}{RT^*}} = \frac{PA_t}{c^*}, \tag{2.30}$$

where γ is the specific heat ratio of air, T^* [K] is the temperature at the throat and c^* [m/s] is the characteristic velocity of the gas inside the control volume. Using (2.29) and (2.30), it is obtained that

$$\dot{P} = c_1\dot{m}_{in} - c_2PA_t = M - c_2PA_t, \tag{2.31}$$

where $c_1 = \frac{RT}{V}$, $c_2 = \frac{c_1}{c^*}$ and $M = c_1\dot{m}_{in}$.

2.2.2 Actuator

The same actuator is used in cold air testing setup as in gas generator, which is a brushless direct current motor, its driver and an encoder. With the aforementioned experimental time delay (in Section 2.1.2), actuator dynamics is given as

$$W_{act}(s) = \frac{\theta(t)}{\theta_{com}(t)} = \frac{e^{-\tau s}}{\tau_{act}s + 1} \tag{2.32}$$

where θ [quadrature] is the realized rotational position of the rotor while θ_{com} [quadrature] is commanded rotational position (4000 quadratures (qc) correspond

to 1 rotation), τ_{act} is actuator closed loop time constant and τ is the time delay in seconds.

2.2.3 Valve Geometry and Drive-Train Elements

The drive-train elements consist of a gear box and a spindle to convert the rotational motion of the motor into the translational motion of a pintle at the throat area (see Fig. 2.9). The linear position of the pintle determines the throat opening.

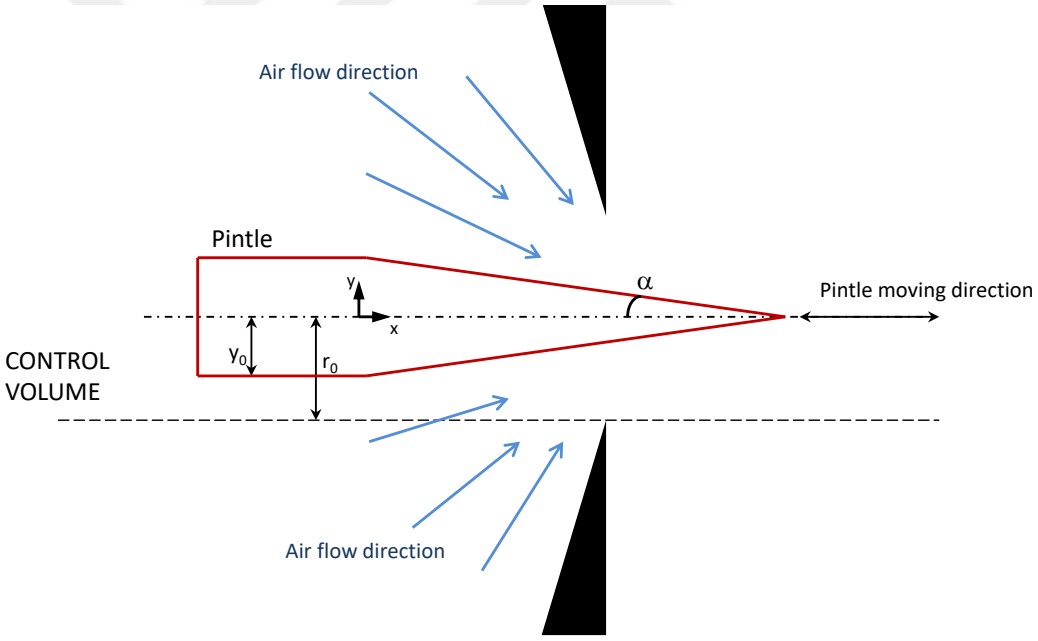

Figure 2.9: Valve geometry

The pintle has one degree of freedom in x direction and open throat area changes as the pintle moves along the x axis due to its conical surface. The cross sectional area of the cylindrical part at the back of the pintle is smaller than the fixed throat area, which makes sure that the open throat area A_t is always larger than zero and protects the system from rapid pressure build up. Below, we provide the valve and the drive train models.

2.2.3.a Valve Geometry in Pintle Element Case

There exist a nontrival relationship between the movement of the pintle and the minimum throat area, where the choked flow conditions occur, due to their complex geometries [49, 51]. The size and the location of the minimum throat area is hard to estimate analytically due to the fact that location of the choked flow line, where the throat area is minimum, shifts towards the upstream as the pintle moves into the throat [51]. In this study, the size of the open throat area is approximated as the projection of the real area on the vertical surface that is perpendicular to the pintle center line. Movement of the pintle along the x [m] axis reduces the projected throat area by

$$y = y_0 - tan(\alpha)x, \tag{2.33}$$

where y_0 [m] is the radius of the pintle at cylindrical part and α [deg] is the half of the cone angle at the tip of the pintle (see Fig. 2.9). The projected open throat area, A_t [m^2], is then calculated as

$$A_t = (r_0^2 - y^2)\pi \tag{2.34}$$

where r_0 [m] is the radius of fully open throat.

2.2.3.b Drive-Train Elements

A gear box with a reduction ratio of $1 : R_1$ is used to increase the torque output of the actuator. The spindle has an R_2 [m] thread pitch, i.e. one turn of rotation corresponds to R_2 [m] translational motion. Therefore, the relationship between the actuator rotational position, θ [quadrature], and the linear position of the pintle, x [m], can be calculated as

$$x = \frac{\theta R_2}{R_1 \times 4000} \tag{2.35}$$

where 4000 quadratures correspond to 1 rotation.

Using (2.33-2.35), it is obtained that

$$A_t = (a_1 + a_2\ \theta + a_3\ \theta^2)\pi \tag{2.36}$$

where $a_1 = r_0^2 - y_0^2$, $a_2 = \frac{2y_0 tan(\alpha) R_2}{R_1 \times 4000}$ and $a_3 = -(\frac{tan(\alpha) R_2}{R_1 \times 4000})^2$.

2.2.4 Model Enhancements Using Experimental Data

To improve the fidelity of the system model, open loop experimental tests are performed and the obtained experimental data is used to adjust model parameters. Firstly, actuator model is updated: Brushless DC motor is commanded

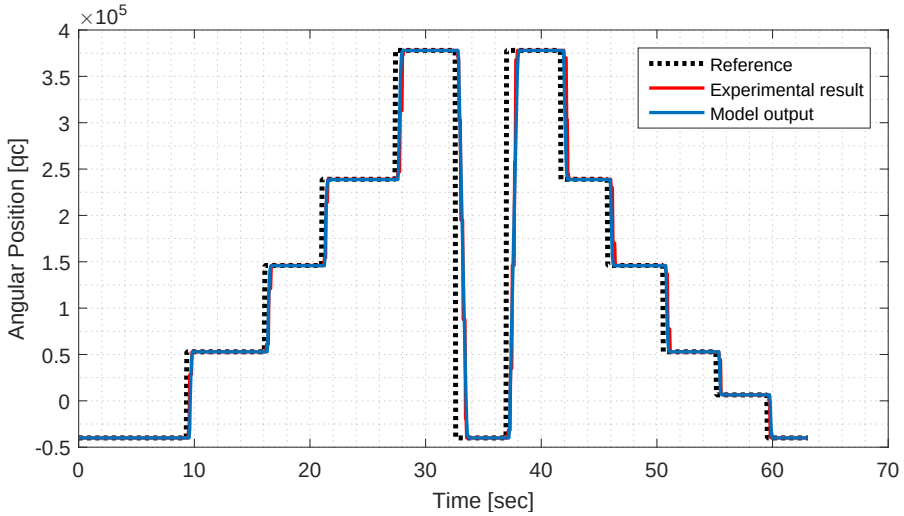

Figure 2.10: Open loop test results and updated model results of the actuator

to track inputs in the position controller mode and based on the response of the actuator the time constant τ_{act} in (2.10) and (2.32) is updated. Experiments also revealed that a considerable amount of time delay exists in the actuator control loop, which is due to the communication and computation lags. After adjusting the time constant and incorporating a time delay, the enhanced actuator model output is compared with the experimental results and the outcomes are presented in Fig. 2.10, which shows that the updated model has a good agreement with the test data. To improve the system model further, parameters in (2.31) are considered next: R, T, V and c^* are available for the test conditions with good accuracy, and therefore the values of these parameters are easily obtained. However mass flow rate ($\dot{m}_{in}$) is not always feasible to measure, especially for relatively small flow rate values. Therefore, the mass flow rate going into the CATS plant

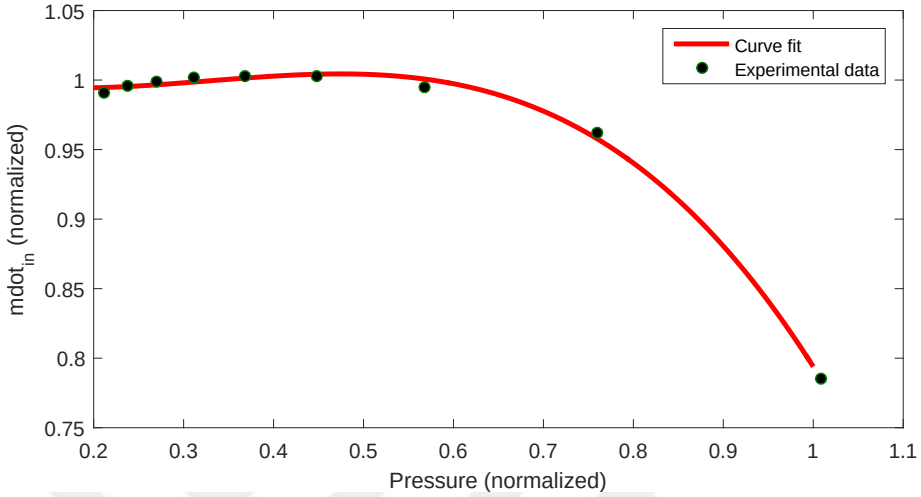

Figure 2.11: $\dot{m}_{in}$ calculated from (2.31) in tests and curve fitted to the data (2.37)

is calculated via (2.31) using steady state pressure values at different operating points and corresponding throat areas. Several values for $\dot{m}_{in}$ at different operating points are plotted in Fig. 2.11 together with a polynomial fit. At low plant pressure, mass flow rates are nearly constant. However, mass flow rate decreases at higher pressure, because high back pressure overcomes the mechanical force in the pressure regulator and reduces the flow rate. Using the polynomial that is fitted to the data in Fig. 2.11, (2.31) is updated as

$$\dot{P} = c_1(c_3P^3 + c_4P^2 + c_5P + c_6) - c_2PA_t. \tag{2.37}$$

Open loop simulation results with the overall updated system model along with experimental results, which are obtained for a range of operating points, are given in Fig. 2.12. It is noted that the model enhancements can be improved further by making comparisons at several other operating points followed by further tuning of the parameters but it is determined that this level of fidelity is enough for simulation evaluation purposes.

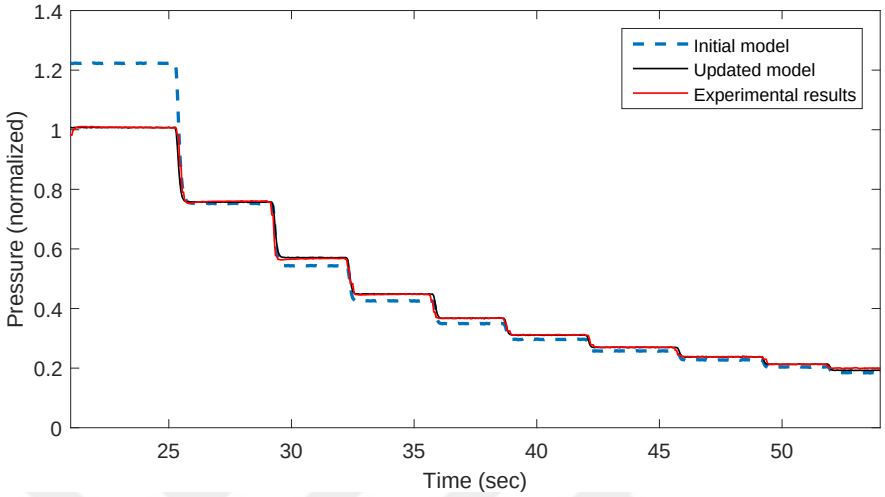

Figure 2.12: Open loop responses of experimental setup and simulation with initial plant model (2.31) and updated plant model (2.37)

2.2.5 Modeling for Controller Design

As explained earlier, the nonlinear model of the CATS developed in the earlier sections is used to evaluate controller alternatives in the simulation environment. To facilitate the controller design, a simpler model is developed following the steps listed below:

- Nonlinear plant model and valve equation in (2.31) and (2.36), respectively, are linearized.
- Actuator dynamics are ignored due to small time constants compared to the plant.
- Inverse of the valve dynamics is inserted in the open loop to cancel its effect.

Linearizing (2.31) around an equilibrium point $(P, A_t) = (P_0, A_{t0})$, it is obtained that

$$\dot{P} = \Delta\dot{P} = (-c_2 A_{t0})\Delta P - (c_2 P_0)\Delta A_t. \tag{2.38}$$

where $\Delta P = P - P_0$ and $\Delta A_t = A_t - A_{t0}$. Defining $a_p \equiv -c_2 A_{t0}$ and $b_p \equiv -c_2 P_0$, (2.38) can be rewritten as

$$\Delta \dot{P} = a_p \Delta P + b_p \Delta A_t. \tag{2.39}$$

When the actuator time constant τ_{act}, (2.32), is obtained using open loop experiments, it is revealed that it can be neglected compared to gas generator pressure dynamics due to being much faster. Therefore, we ignore the first order actuator dynamics for controller design, but keep the time delay, τ, into consideration, which yields an equation of

$$\frac{\theta(t)}{\theta_{com}(t)} = e^{-\tau s}. \tag{2.40}$$

The value of a_3 in (2.36) is much smaller than a_1 and a_2 for meaningful physical parameters, and therefore (2.36) is approximated as

$$A_t \approx (a_1 + a_2\ \theta)\pi. \tag{2.41}$$

It is noted that the valve equation (2.41) is used to convert the required throat area determined by the pressure controller to the required actuator rotational position, which is provided to the actuator as a reference (see Fig. 2.2). Therefore, together with the actuator time lag, τ, the system model used to develop the controller is obtained that

$$W_p(s) = \frac{\Delta P(t)}{\Delta A_{t,com}(t)} = \frac{b_p e^{-s\tau}}{s - a_p} \tag{2.42}$$

Chapter 3

Controller

In this chapter, controller designs for both the gas generator (GG) and the cold air test setup (CATS) are explained.

The structure of the closed loop control system of a conventional throttleable ducted rocket is provided in Fig. 1.4b. The outer loop determines the required gas generator (GG) pressure to obtain a desired thrust/speed profile, and the required pressure becomes the reference for the inner loop pressure controller. The pressure controllers for both the GG and CATS are the focus of this study and these controllers are referred to as "the controller" in the following sections. 4 different controllers are designed: Model reference adaptive controller (MRAC), closed loop reference model (CRM) adaptive controller, the delay resistant closed loop reference model (DR-CRM) adaptive controller and a proportional-integral (PI) controller. These controllers are explained below in the given order. Same controller methodologies are utilized for both GG and CATS with the plant dynamics given in Sections 2.1.4 and 2.2.5.

The mathematical models of plants are obtained using certain assumptions (see Sections 2.1 and 2.2) and they are simplified to facilitate the controller design. These assumptions and simplifications introduce uncertainty to the models

along with inherent disturbances such as metallic particles, deposition or ablation at the throat due to high temperature for the GG and changes in the mass flow rate at the inlet port for CATS. Controllers need to be robust enough to stabilize the closed loop system and provide a desired performance against all uncertainties and disturbances. PI controller, for example, is designed to have a certain amount of phase margin, which can be regarded as a measure of robustness, while its integral action takes care of the disturbances. Adaptive controllers are enforced with a robustfying modification called as the projection algorithm, which is utilized to ensure the boundedness of the controller parameters. Furthermore, disturbances are addressed by inserting integration action. A step-by-step design procedure for the adaptive controller is provided to facilitate the implementation. Finally, controllers' performances are comparatively evaluated using numerical simulations.

It is noted that even though the simplified models obtained for the controller design are found to be first order, adaptive controllers are explained for an n^{th} order single input single output system to address a more general control problem. Controller design for first order systems are given in Section 3.5.

3.1 Model Reference Adaptive Controller (MRAC)

Consider following plant dynamics

$$y_p(t) = W_p(s)u(t), \quad W_p(s) = \frac{k_p Z_p(s)}{R_p(s)}, \tag{3.1}$$

where $y_p \in \Re$ and $u \in \Re$ are the measured output and the control input of the system, respectively. $Z_p(s)$ and $R_p(s)$ are monic polynomials with orders of m and n and $k_p \in \Re$ is the constant gain of the plant. Following assumptions are made for the plant [57]:

- System order n is known along with the relative degree $n^* = n - m$.
- Sign of k_p is known.

- Polynomial $Z_p(s)$ is Hurwitz.

The reference model, which gives the desired response of the closed loop system, is given as

$$y_m(t) = W_m(s)r(t), \quad W_m(s) = \frac{k_m Z_m(s)}{R_m(s)}, \tag{3.2}$$

where $y_m \in \Re$ and $r \in \Re$ are the output of the reference model and bounded reference signal, respectively. $W_m(s)$ is chosen as strictly positive real with relative degree equal to the relative degree of the plant.

State space description of the plant and the signal generators for the output feedback problem with controllable (Λ, b_λ) pair are given as

$$\begin{aligned} \dot{x}_p(t) &= A_p x_p(t) + b_p u(t), \qquad y_p(t) = h_p^T x_p(t) \\ \dot{\omega}_1(t) &= \Lambda \omega_1(t) + b_\lambda u(t) \\ \dot{\omega}_2(t) &= \Lambda \omega_2(t) + b_\lambda y_p(t) \end{aligned} \tag{3.3}$$

where $x_p \in \Re^n$, $\omega_1 \in \Re^{n-1}$, $\omega_2 \in \Re^{n-1}$, $A_p \in \Re^{n\times n}$, $b_p \in \Re^n$, $h_p \in \Re^n$, $\Lambda \in \Re^{(n-1)\times(n-1)}$ is Hurwitz and $b_\lambda \in \Re^{n-1}$.

It can be shown there exist constant parameters $\theta_0 \in \Re$, $\theta_1 \in \Re^{n-1}$, $\theta_2 \in \Re^{n-1}$ and $\theta_r \in \Re$ such that the controller given as

$$u(t) = \theta_0 y_p(t) + \theta_1^T \omega_1(t) + \theta_2^T \omega_2(t) + \theta_r r(t) \tag{3.4}$$

satisfies the desired reference model response characteristics [57]. When the plant parameters are unknown, for $n^* = 1$, the following adaptation law

$$\dot{\Theta}(t) = -\Gamma \text{sign}(k_p) e_1(t) \Omega(t) \tag{3.5}$$

where

$$\Theta(t) = \begin{bmatrix} \theta_0(t) \\ \theta_1(t) \\ \theta_2(t) \\ \theta_r(t) \end{bmatrix}, \quad \Omega(t) = \begin{bmatrix} y_p(t) \\ \omega_1(t) \\ \omega_2(t) \\ r(t) \end{bmatrix}, \tag{3.6}$$

$e_1(t) = y_p(t) - y_m(t)$ is the tracking error, $\Gamma \in \Re^{2n\times 2n}$ is a diagonal matrix with positive elements, stabilizes the closed loop system and ensures that $e_1 \to 0$ as $t \to \infty$ [57].

3.2 Closed Loop Reference Model (CRM) Adaptive Controller

The reference model in the classical model reference adaptive control (3.2) is unaffected by the tracking error. In CRM adaptive controller, however, the tracking error $e_1(t) = y_p(t) - y_m(t)$ is fed back to the reference model for the purpose of improving the transient dynamics [26]. Consider the following state space representation of the reference model dynamics from (3.2) as

$$\dot{x}_m(t) = A_m x_m(t) + b_m r(t), \quad y_m(t) = h_m^T x_m(t), \tag{3.7}$$

where $A_m \in \Re^{n\times n}$, $b_m \in \Re^n$ and $h_m \in \Re^n$. In classical model reference adaptive control, A_m, b_m and h_m are chosen such that the transfer function $h_m^T(sI - A_m)b_m = W_m(s) = k_m \frac{Z_m(s)}{R_m(s)}$ becomes strictly positive real. In CRM adaptive controller, the reference model is modified as

$$\dot{x}_m(t) = A_m x_m(t) + b_m r(t) + L(y_p(t) - y_m(t)), \quad y_m(t) = h_m^T x_m(t), \tag{3.8}$$

where $L \in \Re^n$ is a design parameter vector. The relationship between the reference model output y_m, the reference r and the tracking error e_1 then becomes

$$y_m(t) = W_m(s)r(t) + W_L(s)e_1(t) \tag{3.9}$$

where

$$h_m^T(sI - A_m)L = k_L \frac{Z_L(s)}{R_m(s)} = W_L(s). \tag{3.10}$$

Polynomial $Z_L(s)$ is order of $n-1$. Boundedness of all the signals in the closed loop system along with the convergence of the tracking error as in classical MRAC is valid for the CRM approach, using the same controller structure (3.4) and the adaptive law (3.5), as long as L is chosen such that the transfer function

$$W_e = \frac{Z_m(s)}{R_m(s) - k_L Z_L(s)} \tag{3.11}$$

is strictly positive real (see [43]).

3.3 Delay Resistant Closed Loop Reference Model (DR-CRM) Adaptive Controller

Consider the following plant with an input time delay

$$y_p(t) = k_p \frac{Z_p(s)}{R_p(s)} u(t-\tau) = W_p(s)u(t-\tau) \tag{3.12}$$

where $y_p \in \Re$ is the measured output, $u \in \Re$ is the control signal, τ is the known time delay, $Z_p(s)$ and $R_p(s)$ are monic coprime polynomials with orders of m and n, respectively, and $k_p \in \Re$ is the constant gain of the plant. Following assumptions are made for the plant:

- System order n is known along with the relative degree $n^* = n - m$.
- Sign of k_p is known.
- Polynomial $Z_p(s)$ is Hurwitz.

The reference model dynamics are given with the closed loop reference model structure as

$$\begin{aligned} \dot{x}_m(t) &= A_m x_m(t) + b_m r(t-\tau) + L(y_p(t) - y_m(t)) \\ y_m(t) &= h_m^T x_m(t) \end{aligned} \tag{3.13}$$

where $x_m \in \Re^n$, $y_m \in \Re$, $r \in \Re$, $A_m \in \Re^{n\times n}$ and $b_m, L, h_m \in \Re^n$. Input-output relationship of the closed loop reference model is given as

$$y_m(t) = W_m(s)r(t-\tau) + W_L(s)e_1(t) \tag{3.14}$$

where $e_1 = y_p - y_m$ is the tracking error. The transfer functions describing the closed loop reference model are

$$\begin{aligned} h_m^T(sI - A_m)b_m &= k_m \frac{Z_m(s)}{R_m(s)} = W_m(s) \\ h_m^T(sI - A_m)L &= k_L \frac{Z_L(s)}{R_m(s)} = W_L(s) \end{aligned} \tag{3.15}$$

where $R_m(s)$ is a monic polynomial with order n while $Z_m(s)$ and $Z_L(s)$ are two monic polynomials with order $n-1$, $k_m \in \Re$ and $k_L \in \Re$ are the gains of the transfer functions. It is noted that under model matching conditions the tracking error becomes zero, which reduces the reference model (3.14) to

$$y_m(t) = W_m(s)r(t-\tau). \tag{3.16}$$

State space description of the plant (3.12) and the signal generators for the output feedback problem with the controllable (F, g) pair are given as

$$\begin{aligned} \dot{x}_p(t) &= A_p x_p(t) + b_p u(t-\tau), \quad y_p(t) = h_p^T x(t) \\ \dot{\omega}_1(t) &= F\omega_1(t) + gu(t-\tau) \\ \dot{\omega}_2(t) &= F\omega_2(t) + gy_p(t) \end{aligned} \tag{3.17}$$

where $x_p \in \Re^n$ is the state vector, $\omega_1, \omega_2 \in \Re^n$, $A_p \in \Re^{n\times n}$, b_p, $h_p \in \Re^n$, $F \in \Re^{n\times n}$ is Hurwitz and $g \in \Re^n$. It can be shown that there exists constant controller parameters $\beta_1^* \in \Re^n$, $\beta_2^* \in \Re^n$ and $k^* \in \Re$ such that the controller

$$u(t) = \beta_1^{*T}\bar{\omega}_1(t) + \beta_2^{*T}\bar{\omega}_2(t) + k^* r(t) \tag{3.18}$$

where $\bar{\omega}_1(t) \triangleq \omega_1(t+\tau)$, $\bar{\omega}_2(t) \triangleq \omega_2(t+\tau)$ together with the rewritten plant dynamics

$$\begin{aligned} \dot{\bar{x}}_p(t) &= A_p\bar{x}_p(t) + b_p u(t), \quad \bar{y}_p(t) = h_p^T\bar{x}_p(t) \\ \dot{\bar{\omega}}_1(t) &= F\bar{\omega}_1(t) + gu(t) \\ \dot{\bar{\omega}}_2(t) &= F\bar{\omega}_2(t) + g\bar{y}_p(t) \end{aligned} \tag{3.19}$$

where $\bar{x}_p(t) \triangleq x_p(t+\tau)$ and $\bar{y}_p(t) \triangleq y_p(t+\tau)$, satisfies the model matching conditions [25].

It is shown in [57] that the plant output, $y_p(t)$, can be expressed as a linear combination of $\omega_1(t), \omega_2(t)$ as

$$y_p(t) = c^T\omega_1(t) + d^T\omega_2(t) \tag{3.20}$$

where $c, d \in \Re^n$. When (3.20) is substituted into (3.17), it is obtained that

$$\begin{bmatrix} \dot{\omega}_1(t) \\ \dot{\omega}_2(t) \end{bmatrix} = A \begin{bmatrix} \omega_1(t) \\ \omega_2(t) \end{bmatrix} + bu(t-\tau), \tag{3.21}$$

where $A \in \Re^{2n\times 2n}$ and $b \in \Re^{2n}$ are given as $A = \begin{bmatrix} F & 0 \\ gc^T & F+gd^T \end{bmatrix}$ and $b = \begin{bmatrix} g \\ 0 \end{bmatrix}$. Non-casual terms in (3.18) can then be calculated as

$$\begin{bmatrix} \bar{\omega}_1(t) \\ \bar{\omega}_2(t) \end{bmatrix} = e^{A\tau} \begin{bmatrix} \omega_1(t) \\ \omega_2(t) \end{bmatrix} + \int_{-\tau}^{0} e^{A\eta} b u(t+\eta) d\eta. \tag{3.22}$$

When (3.22) is substituted into (3.18), the control signal becomes

$$u(t) = \alpha_1^{*T}\omega_1(t) + \alpha_2^{*T}\omega_2(t) + \int_{-\tau}^{0} \phi^*(\eta) u(t+\eta) d\eta + k^* r(t) \tag{3.23}$$

where $\alpha_{1,2}^* \in \Re^n$, $\phi^*(\eta) \in \Re$ are the corresponding controller parameters which eliminate the non-causality in controller (3.18) using (3.22).

In the case of unknown plant parameters, the control input, $u(t)$, can be split into two sub-signals as

$$u(t) = u_1(t) + u_2(t) \tag{3.24}$$

where

$$u_1(t) = \alpha_1^{*T}\omega_1(t) + \alpha_2^{*T}\omega_2(t) + \int_{-\tau}^{0} \phi^*(\eta) u(t+\eta) d\eta + k^* r(t) \tag{3.25}$$

and

$$u_2(t) = \tilde{\alpha}_1^T(t)\omega_1(t) + \tilde{\alpha}_2^T(t)\omega_2(t) + \int_{-\tau}^{0} \tilde{\phi}(t,\eta) u(t+\eta) d\eta + \tilde{k}(t) r(t) \tag{3.26}$$

where $\tilde{\alpha}_i(t) = \alpha_i(t) - \alpha_i^*$ for $i = 1, 2$; $\tilde{\phi}(t,\eta) = \phi(t,\eta) - \phi^*(\eta)$ and $\tilde{k}(t) = k(t) - k^*$.

Substituting (3.24), using (3.25) and (3.26), into (3.17), the closed loop dynamics is obtained as

$$\begin{aligned} \dot{X}_p(t) &= A_{mn} X_p(t) + b_{mn}\left[\tilde{\theta}(t-\tau) w(t-\tau) + \int_{-\tau}^{0} \tilde{\phi}(t-\tau,\eta) u(t-\tau+\eta) d\eta + k^* r(t-\tau)\right] \\ y_p(t) &= h_{mn}^T X_p(t) \end{aligned} \tag{3.27}$$

where $A_{mn} = \begin{bmatrix} A_p & b_p\beta_1^* & b_p\beta_2^* \\ 0 & F+g\beta_1^* & g\beta_2^* \\ gh_p^T & 0 & F \end{bmatrix}$, $b_{mn} = \begin{bmatrix} b_p \\ g \\ 0 \end{bmatrix}$, $h_{mn}^T = \begin{bmatrix} h_p^T & 0 & 0 \end{bmatrix}$, $X_p(t) = \begin{bmatrix} x_p^T(t) & \omega_1^T(t) & \omega_2^T(t) \end{bmatrix}^T$, $w(t) = \begin{bmatrix} \omega_1^T(t) & \omega_2^T(t) & r(t) \end{bmatrix}^T$ and $\tilde{\theta}(t) = \begin{bmatrix} \tilde{\alpha}_1(t) & \tilde{\alpha}_2(t) & \tilde{k}(t) \end{bmatrix}$.

It is noted that when the parameter errors are zero, i.e. $\tilde{(\cdot)} = 0$, the closed loop dynamics represented by (3.27) becomes equivalent to that of the reference model dynamics (3.16), which shows that the system formed by (A_{mn}, b_{mn}, h_{mn}) is a non-minimal representation of the reference model:

$$h_{mn}^T(sI - A_{mn})b_{mn} \equiv k_p \frac{Z_m(s)}{R_m(s)} = \frac{k_p}{k_m} W_m(s). \tag{3.28}$$

Using (3.27) and (3.28), the plant output is obtained as

$$y_p(t) = \frac{k_p}{k_m} W_m(s) \left[\tilde{\theta}(t-\tau)w(t-\tau) + \int_{-\tau}^{0} \tilde{\phi}(t-\tau,\eta)u(t-\tau+\eta)d\eta + k^* r(t-\tau) \right]. \tag{3.29}$$

Subtracting (3.14) from (3.29), it can be obtained as

$$e_1(t) = \frac{k_p}{k_m} W_m(s) \left[\tilde{\theta}(t-\tau)w(t-\tau) + \int_{-\tau}^{0} \tilde{\phi}(t-\tau,\eta)u(t-\tau+\eta)d\eta \right] - W_L e_1(t). \tag{3.30}$$

Solving (3.30), the tracking error can be found as

$$e_1(t) = k_p \frac{Z_m(s)}{R_m(s) - k_L Z_L(s)} \left[\tilde{\theta}(t-\tau)w(t-\tau) + \int_{-\tau}^{0} \tilde{\phi}(t-\tau,\eta)u(t-\tau+\eta)d\eta \right] \tag{3.31}$$

where $\frac{Z_m(s)}{R_m(s)-k_L Z_L(s)} = W_e(s)$ has sufficient degrees of freedom, in terms of the design parameter vector L, to be determined as a SPR transfer function (see Section 3.2).

The closed loop reference model in (3.13) can be rewritten as,

$$\begin{aligned} \dot{x}_{mn}(t) &= A_{mn}x_{mn}(t) + b_{mn}k^* r(t-\tau) + GL(y_p(t) - y_m(t)) \\ y_m(t) &= h_{mn}^T x_{mn}(t) \end{aligned} \tag{3.32}$$

for $x_{mn} = \begin{bmatrix} x_p^{*T}(t) & \omega_1^{*T}(t) & \omega_2^{*T}(t) \end{bmatrix}^T$ where $x_p^*(t)$, $\omega_1^*(t)$ and $\omega_2^*(t)$ are the signals in the reference model, corresponding to the signals $x_p(t)$, $\omega_1(t)$ and $\omega_2(t)$ in the closed loop dynamics, respectively. $G \in \Re^{3n \times n}$ is the constant matrix to transform x_m to the controllable subspace in x_{mn} (see [43]). Error dynamics, $e(t) = X_p(t) - x_{mn}(t)$, in non-minimal form, is found by subtracting (3.32) from

(3.27) as

$$\dot{e}(t) = A_e e(t) + b_{mn}\left[\tilde{\theta}(t-\tau)w(t-\tau) + \int_{-\tau}^{0} \tilde{\phi}(t-\tau,\eta)u(t-\tau+\eta)d\eta\right] \qquad (3.33)$$
$$e_1(t) = h_{mn}^T e(t)$$

where

$$A_e = A_{mn} - GLh_{mn}^T. \qquad (3.34)$$

It can be shown [25], utilizing the error dynamics (3.33), that the controller (3.24)-(3.26), along with the adaptation laws given as

$$\begin{aligned} \dot{\tilde{\theta}}(t) = \dot{\theta}(t) &= -\text{sign}(k_p)\Gamma_\theta e_1(t)\omega(t-\tau) \\ \dot{\tilde{\phi}}(t,\eta) = \dot{\phi}(t) &= -\text{sign}(k_p)\Gamma_\phi e_1(t)u(t-\tau+\eta) \quad -\tau \le \eta \le 0 \end{aligned} \qquad (3.35)$$

stabilizes the closed loop system as long as L is chosen to ensure that $W_e(s)$ is SPR. Furthermore, tracking error $e_1(t)$ converges to zero. $\Gamma_\theta \in \Re^{(2n+1)\times(2n+1)}$ is a diagonal matrix with positive elements and $\Gamma_\phi \in \Re^+$.

3.4 Proportional-Integral (PI) Controller

The controller transfer function is

$$G_{PI}(s) = K_p + \frac{K_i}{s} \qquad (3.36)$$

where scalar controller parameters K_p and K_i are selected to make the closed loop dynamics provide a similar response with the reference model (3.2) selected for MRAC.

In PI controller design, delay free part of the plant models (2.28) and (2.42) are used. Constant coefficients c_8, c_9, b_p and a_p are found using experimental data. Equilibrium points around which the nonlinear plant dynamics are linearized (A_{t0}, P_{g0}) are given in Table 3.1 along with the controller gains.

Selection of controller gains are carried out using frequency-response methodology. Frequency response plots of the selected reference model for MRAC and

Table 3.1: Plant parameters and PI controller gains

System	Equilibrium point		Plant parameters		Controller gains	
	P_{g0}	A_{t0}	a_p or c_8	b_p or c_9	K_p	K_i
Gas generator	40 bar	75,6 mm^2	-2,94	-2,19	-1,5	-4,7
Cold air testing system	15 bar	14,27 mm^2	-11,67	-12,26	-0,25	-3,4

the compensated systems with PI controllers are provided in Fig. 3.1, where it is seen that the closed loop systems compensated by the PI controller have similar response with the MRAC reference model.

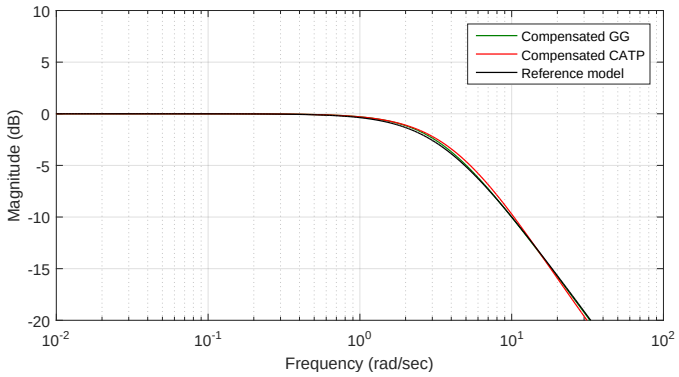

(a) Magnitude

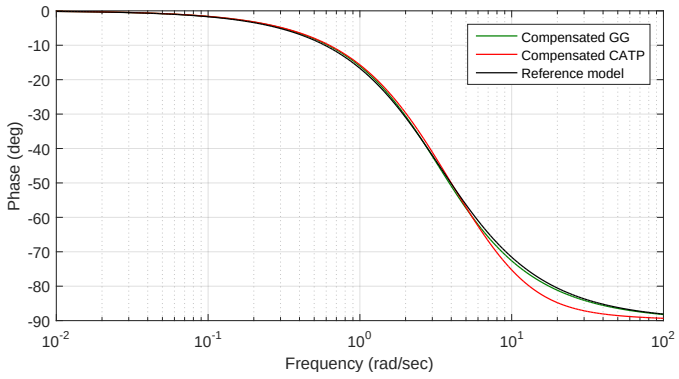

(b) Phase

Figure 3.1: Comparison of the Bode plots of the compensated closed loop systems with the designed PI controllers and the reference model

3.5 Implementation Enhancements

The implementation of the adaptive controllers requires some modifications to address the issues that were not taken into consideration during the initial design but arise in real experimental tests. Below, these experimental requirements and how they are addressed are explained.

3.5.1 Disturbance Rejection

The disturbances, while designing adaptive controllers, are not explicitly taken into account. In throttleable ducted rocket propulsion systems, however, the solid propellant in the gas generator contains metallic particles (see Fig. 1.1), which can cause deposition or ablation at the throat between the gas generator and the ram combuster, which acts like an additive disturbance on the effective throat area. Therefore, it is important to incorporate disturbance rejection capabilities into the gas generator pressure controller. Since the plant models (2.28) and (2.42), which are developed for the controller design, are of first order, the disturbance rejection modification explained below utilizes a scalar plant model.

Consider the plant

$$\dot{y}_p(t) = a_p y_p(t) + b_p(u(t) + d_0) \tag{3.37}$$

where y_p is the system output, d_0 is the unknown constant disturbance, u is the plant input and a_p and b_p are the plant parameters. An additional adaptive controller parameter, $\theta_3(t)$, is introduced to the controller structure for MRAC and CRM adaptive controller, which results in the following control signal

$$u(t) = \theta_0(t)y_p(t) + \theta_r(t)r(t) + \theta_3(t) \tag{3.38}$$

where θ_0, θ_r and θ_3 are the adaptive control parameters to be determined and r is a bounded reference signal. The adaptation laws for the controller parameters are given as

$$\dot{\bar{\Theta}}(t) = -\text{sign}(b_p)\bar{\Gamma}e_1(t)\bar{\Omega}(t) \tag{3.39}$$

where $\bar{\Theta}^T(t) = \begin{bmatrix}\theta_0(t) & \theta_r(t) & \theta_3(t)\end{bmatrix}$, $\bar{\Omega}^T = \begin{bmatrix}y_p(t) & r(t) & 1\end{bmatrix}$, $\bar{\Gamma} > 0$ is the diagonal adaptation rate matrix and e_1 is the tracking error given by $e_1 = y_p - y_m$. The reference model for the MRAC is appointed as

$$\dot{y}_m(t) = a_m y_m(t) + b_m r(t), \tag{3.40}$$

and the reference model for CRM adaptive controller is selected as,

$$\dot{y}_m(t) = a_m y_m(t) + b_m r(t) + l(y_p(t) - y_m(t)), \tag{3.41}$$

where $a_m, b_m, l \in \Re$, $a_m = -b_m$ for unity DC gain and $a_m < 0$ and $l > 0$. It is noted that for a first order plant, choosing $l > 0$ satisfies the stability conditions.

Similarly, DR-CRM adaptive control signal is modified as

$$u(t) = \alpha_y(t) y_p(t) + \int_{-\tau}^{0} \lambda(t,\eta) u(t+\eta) d\eta + k(t) r(t) + \theta_3(t). \tag{3.42}$$

The adaptive laws for the controller parameters $\alpha_y, \lambda, k, \theta_3 \in \Re$ are given as

$$\begin{aligned} \dot{\theta}(t) &= -\text{sign}(b_p)\Gamma_\theta e_1(t)\omega(t-\tau) \\ \frac{\partial \lambda}{\partial t}(t,\eta) &= -\text{sign}(b_p)\gamma_\lambda e_1(t) u(t+\eta-\tau) \quad -\tau \le \eta \le 0 \end{aligned} \tag{3.43}$$

where $\theta^T(t) = \begin{bmatrix}\alpha_y(t) & k(t) & \theta_3(t)\end{bmatrix}$, $\omega^T(t) = \begin{bmatrix}y_p(t) & r(t) & 1\end{bmatrix}$, $\Gamma_\theta > 0$ and $\gamma_\lambda \in \Re^+$ are adaptation rate constants.

The reference model for the DR-CRM adaptive controller is determined as

$$\dot{y}_m(t) = a_m y_m(t) + b_m r(t-\tau) + l(y_p(t) - y_m(t)), \tag{3.44}$$

where $a_m, b_m, l \in \Re$, $a_m = -b_m$ for unity DC gain and $a_m < 0$ and $l > 0$.

3.5.2 Robustness

The design of the adaptive controllers presented in Sections 3.1, 3.2 and 3.3 portrayed an idealized case, where the delay free part of the plant dynamics are assumed to be linear and time-invariant with unknown but constant parameters.

Furthermore, the measurements are assumed to be perfect. However, it is known that in reality, no plant is truly linear or finite dimensional. Parameters may vary with time and operating conditions, and measurements are always contaminated with noise. The plant model used for the controller design is always an approximation of reality. Therefore, we need a robustfying modification against possible parameter drifts in adaptive controller parameters, due to these non-ideal situations. One common remedy utilized to prevent parameter drift is the projection algorithm [58], which is explained below.

Consider a controller parameter vector $\Theta(t) \in \Re^k$. The upper bound on the controller parameter vector norm $||\Theta||$, to activate the projection modification is defined as $\Theta_{max} \in \Re^+$. A continuous and differentiable convex function $f : \Re^k \rightarrow \Re$ is introduced as

$$f(\Theta) = \frac{||\Theta||^2 - \Theta_{max}^2}{\epsilon \Theta_{max}^2} \tag{3.45}$$

where $\epsilon > 0$ is a constant which defines the projection tolerance region where $||\Theta|| \leq \Theta_{max}(\sqrt{1+\epsilon})$ forms a hard bound on the parameter norm. The projection operator, $\text{Proj} : \Re^k \times \Re^k \rightarrow \Re^k$, is described as

$$\text{Proj}(\Theta, y) \triangleq \begin{cases} y - \frac{\nabla f(\Theta)(\nabla f(\Theta))^T}{||\nabla f(\Theta)||^2} y f(\Theta), & \text{if } ||\Theta|| > \Theta_{max} \ \wedge \ y^T \nabla f(\Theta) > 0 \\ y, & \text{otherwise} \end{cases} \tag{3.46}$$

where $y \in \Re^k$, $\nabla f(\Theta) = \left(\frac{\partial f(\Theta)}{\partial \Theta_1} \cdots \frac{\partial f(\Theta)}{\partial \Theta_k} \right)^T \in \Re^k$ is the gradient vector of f.

The adaptive control law is then modified as

$$\dot{\Theta} = \text{Proj}(\Theta, -\text{sign}(k_p) \Gamma e_1 \Omega) \tag{3.47}$$

where $\Gamma \in \Re^{k \times k}$ is a diagonal matrix with positive elements, $e_1 \in \Re$ is the tracking error, $\Omega \in \Re^k$ is the regressor vector containing system signals. It can be shown that with the adaptive law (3.47) utilizing projection, the parameter drift is prevented [58].

Although we observed in the experiments that the introduction of the projection algorithm prevents parameter drift, there are no well defined procedures to determine the upper bound Θ_{max} on the controller parameter vector Θ. One

method is to calculate this bound using the worst case uncertainty case. Another method is to conduct several experiments without projection and observe the variation of controller parameters, which can help define a reasonable upper bound. A third approach is setting initial values for the controller parameters that would satisfy the matching conditions for the nominal plant dynamics and then determining the upper bound for the parameters as a certain percentage higher than these initial values. The second method is utilized for this study.

3.5.3 Digital Implementation of the Integral Term in DR-CRM Adaptive Controller

For computer implementation purposes, the finite integral term in (3.42) is approximated as,

$$\int_{-\tau}^{0} \lambda(t,\eta)u(t+\eta)d\eta = \sum_{i=1}^{m} \lambda_i(t)u(t-idt) = \bar{\lambda}^T(t)\bar{u}(t) \tag{3.48}$$

where $dt = 50$ ms is the sampling interval of the implemented software, $\tau = 300$ ms is the time delay and $m = \frac{\tau}{dt} = 6$. $\bar{\lambda} \in \Re^m$ is the vector containing parameters $\bar{\lambda}^T(t) = \begin{bmatrix}\lambda_1(t)\cdots\lambda_m(t)\end{bmatrix}$ and $\bar{u} \in \Re^m$ is the delayed input vector $\bar{u}^T(t) = \begin{bmatrix}u(t-dt)\cdots u(t-mdt)\end{bmatrix}$.

Adaptation law (3.43) is updated as

$$\dot{\bar{\theta}}(t) = -\text{sign}(b_p)\bar{\Gamma}_{\bar{\theta}}\, e_1(t)\bar{\omega}(t) \tag{3.49}$$

where

$$\bar{\theta}(t) = \begin{bmatrix}\alpha_y(t)\\ \lambda_1(t)\\ \vdots\\ \lambda_m(t)\\ k(t)\\ \theta_3(t)\end{bmatrix} \quad \bar{\omega}(t) = \begin{bmatrix}y_p(t)\\ u(t-dt)\\ \vdots\\ u(t-mdt)\\ r(t)\\ 1\end{bmatrix} \tag{3.50}$$

and $\bar{\Gamma}_{\bar{\theta}} > 0$ is a diagonal adaptation rate matrix.

3.5.4 Initialization of the Controller Parameters

One way to initialize the adaptive controller is to use initial values that would satisfy model matching for the nominal plant dynamics. However, in MRAC and CRM adaptive controller designs, initial parameters $\theta_0(0)$ and $\theta_r(0)$ had to be lowered to obtain the best performance since the presence of the time delay prevents exact model matching due to the lack of exact delay compensation terms. On the other hand, the initial parameters for DR-CRM adaptive controller are set to satisfy the model matching conditions for the nominal plant dynamics. Initial parameter $\theta_3(0)$ is selected zero for all adaptive controllers.

3.5.5 Selecting the Design Parameters for MRAC

Adaptation rate for a particular parameter θ_i in MRAC is chosen according to the empirical formula [59]

$$\bar{\Gamma}_{ii} = \frac{|\theta_i^*|}{3\tau_m(\bar{r})^2} \tag{3.51}$$

where θ_i^* is the ideal value of the controller parameter, τ_m is the smallest time constant of the reference model and $\bar{r}$ is the maximum possible amplitude of the reference signal which is equal to the amplitude of the operating range. Since the ideal controller parameters, θ_i^*, are assumed to be unknown, nominal values calculated using the matching conditions are used instead.

Adaptation rates obtained from (3.51) are calculated for the worst case scenario which is usually valid at the beginning of the operation when the tracking error and the system states are of the same order of magnitude with the reference signal. Moreover, the calculation (3.51) requires the estimation of the ideal control parameters. Due to these approximations, we include a fine-tuning matrix W for MRAC to fine-tune the adaptation rates as $\bar{\Gamma}_W = \bar{\Gamma}W$ where

$$W = \begin{bmatrix} p_1 & 0 & 0 \\ 0 & p_2 & 0 \\ 0 & 0 & p_3 \end{bmatrix} \tag{3.52}$$

and adjustable constants $p_{1,2,3}$ are used for the fine-tuning process. It was experienced during simulations that selection of $p_1 = p_2 = 1$ and $p_3 > 1$ provide faster and more robust system response.

3.5.6 Selecting the Design Parameters for CRM and DR-CRM Adaptive Controllers

CRM gain, ℓ, helps suppress the oscillations in the case of high adaptation rates. However, a numerically large ℓ can cause so-called "peak phenomena" in non-zero initial tracking error [60]. Therefore, a procedure to determine the optimum value of the CRM gain and adaptation rates is needed to reduce the time and effort spent for the controller tuning. Below steps, inspired from [26], are followed separately for CRM and DR-CRM adaptive controllers:

1. Find the adaptation rates using (3.51) and define the adaptation rate vector, $\bar{\gamma}$.
2. Find the norm of the adaptation rate vector, $||\bar{\gamma}||$.
3. Define the CRM gain, ℓ, equal to $||\bar{\gamma}||$.
4. Increase ℓ and $\bar{\gamma}$ together by keeping $\ell = ||\bar{\gamma}||$ until a desired tracking performance is obtained in numerical simulations.

The same adaptation rate, γ_λ, which is determined through simulations, is chosen for each λ_i since they have same order of magnitude.

3.6 Step by Step Controller Design Procedure

A clear, step by step procedure is provided below to facilitate the adaptive controller design.

Step 1: Determine the reference model dynamics by choosing appropriate (A_m, b_m, h_m) for the performance specifications of the closed loop system. (A_m, b_m, h_m) should form a strictly positive real (SPR) transfer function for MRAC.

Step 2: Signals $\omega_{1,2}(t)$ in (3.3) and (3.17) are generated by choosing (F, g) and (Λ, b_Λ) so that they form controllable pairs. Since these signals operate like state observers, eigenvalues of the matrices F and Λ should be faster than the reference model dynamics. For a first order plant, these signals are not required.

Step 3: Set the initial conditions of the controller parameters using Section 3.5.4.

Step 4: Find the adaptation rates and CRM gain, ℓ, using Section 3.5.5-3.5.6. CRM gain should be selected such that $W_e(s)$ in (3.11) is an SPR transfer function for both CRM and DR-CRM adaptive controllers.

Step 5: Tune the parameters γ_λ and p_3 in (3.50) and (3.52) using numerical simulations and then fine-tune again during experiments.

Step 6: Integrate the projection algorithm provided in (3.47) to the adaptation laws.

All of the adaptive controllers considered in this paper requires minimal amounts of computational resources and memory. DR-CRM, having the highest number of terms in the control signal, for example, needs only 256 bytes of memory for data storage. It has 116 operations per cycle, which corresponds to around 2320 floating point operations per second (flops). See the Appendix A for detailed memory requirement and computational load calculations.

3.7 Simulations

Simulation results are presented in this section for both the gas generator (GG) and the cold air testing setup (CATS) control problems. All the parameters defining the controller (initial conditions of the controller parameters, adaptation

rates and the CRM gain) are obtained using the methods presented in Section 3.6. The reference model is chosen to satisfy the performance specifications listed in Table 3.2 and the Bode plot of the selected reference model is given in Fig. 3.1. The PI controller gains are provided in Table 3.1.

Table 3.2: Specifications of the reference model

Steady state error	Rise time	Settling time (5 %)	Maximum overshoot
0 %	0.6 sec	1.5 sec	10 %

In the cold air testing setup (CATS) case, the enhanced model are used for simulations with the coefficients c_3-c_6 in (2.37) whose values are obtained from the curve fit study presented in Section 2.2.4. In the gas generator control case, the nonlinear model developed in Sections 2.1.1, 2.1.2 and 2.1.3 are used. All parameters in the simulations are given in Table 3.3. It is noted that the same actuator and drive-train elements are used in both the GG and the CATS control problems. Numerical simulations are carried out using Matlab ® with a sampling interval of 50 msec.

Table 3.3: System parameters used in the simulations

Gas generator model			**Cold air testing system model**		
R ($\frac{J}{kg-K}$)	T (K)	ρ (kg/m^3)	R ($\frac{J}{kg-K}$)	T (K)	V (m^3)
297	1400	1472	297	300	$2.5*10^{-4}$
A_b (m^2)	a	c^* (m/s)	c^* (m/s)	c_3	c_4
0.0254	$7.8484*10^{-5}$	1100	435.93	$6.77*10^{-6}$	$2.42*10^{-4}$
n	$V_{g,initial}$ (m^3)	R_{throat} (mm)	c_5	c_6	y_0 (mm)
0.299	$6.845*10^{-3}$	15	$2.5*10^{-3}$	$1.56*10^{-2}$	6.3
r_{pis} (mm)	R_1	R_2 (mm)	r_0 (mm)	α (deg)	R_1
12	14	2	6.5	5	14
τ_{act} (msec)	τ (msec)	Propellant mass (kg)	R_2 (mm)	τ_{act} (msec)	τ (msec)
60	300	6.21	2	60	300

3.7.1 Cold Air Testing System Simulations

Firstly, performance of MRAC is compared with the PI controller. Then, MRAC, CRM adaptive controller and DR-CRM adaptive controller are comparatively

evaluated, where demanding tracking tasks are utilized to reveal the performance differences between these controllers.

3.7.1.a MRAC vs. PI Controller

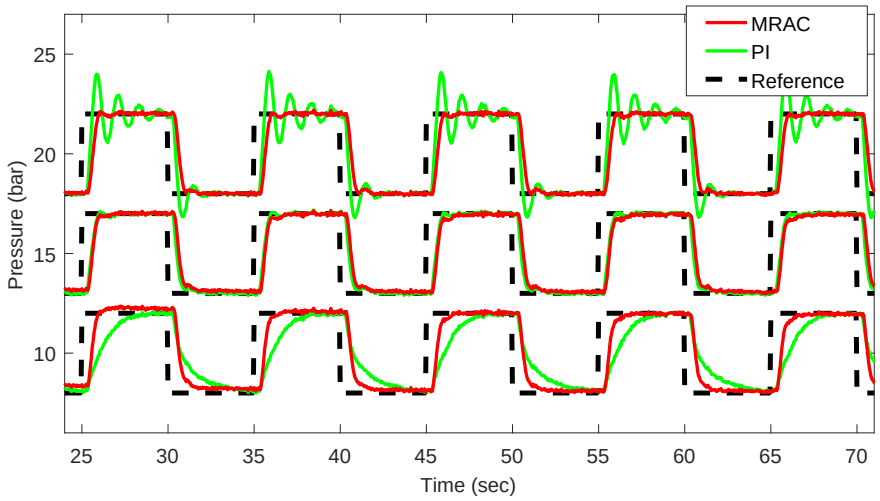

Figure 3.2: Tracking curves in cold air testing system simulation for the PI controller and MRAC at three different operating points.

In Fig. 3.2, simulation results are given demonstrating the performances of MRAC and the PI controller. It is noted that although the PI controller and MRAC show very similar performances around the nominal operating pressure, between 13 and 17 bars, the closed loop system with the PI controller presents an oscillatory response for higher pressure operating conditions and a slow response for lower pressures. On the other hand, MRAC can adapt itself to changing operating conditions and provides a more consistent performance across operating points.

3.7.1.b Comparative Evaluation of Adaptive Controllers

The premise of CRM and delay compensation modifications for the conventional MRAC controller is that they provide higher performance without causing excessive oscillations. To demonstrate the difference that these modifications can

make, more demanding reference trajectories, compared to those of the case presented in Fig. 3.2, are used for the reference tracking tests. Also, time constant of the reference model, τ_m, is halved to obtain a fast response. Adaptation rates of MRAC are updated using (3.51) and a new p_3, employed in (3.52), is obtained empirically. The results of these simulations are given in Fig. 3.3-3.5.

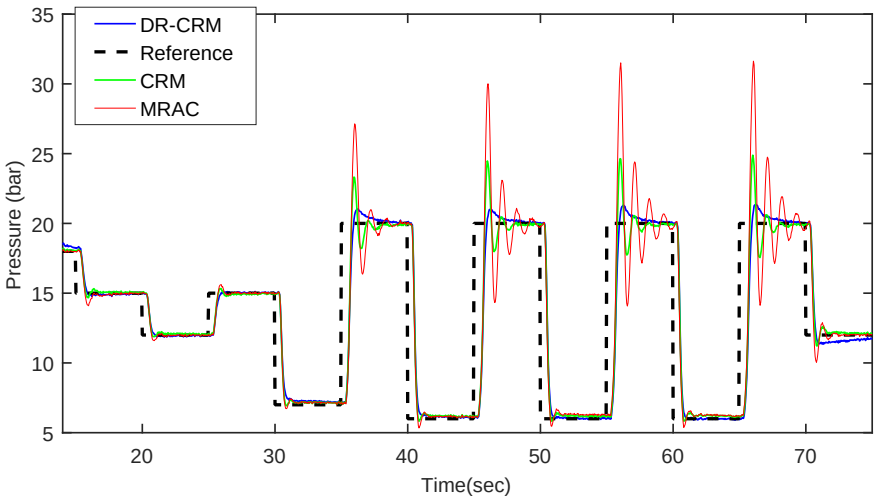

Figure 3.3: Reference tracking of MRAC, CRM adaptive control and DR-CRM adaptive control in simulations.

MRAC, CRM adaptive controller and DR-CRM adaptive controller provide similar performances for small variations in the pressure demand but MRAC response becomes oscillatory once the demanded variation is increased by three times. Although CRM adaptive controller provides a considerably more damped response compared to MRAC, the best response is obtained for the case where DR-CRM adaptive controller is employed. Figure 3.4 shows that DR-CRM controller provides the smoothest control input. In Fig. 3.5, adaptive control parameters are shown where MRAC parameters hit the projection boundary and stays within the projection tolerance limits.

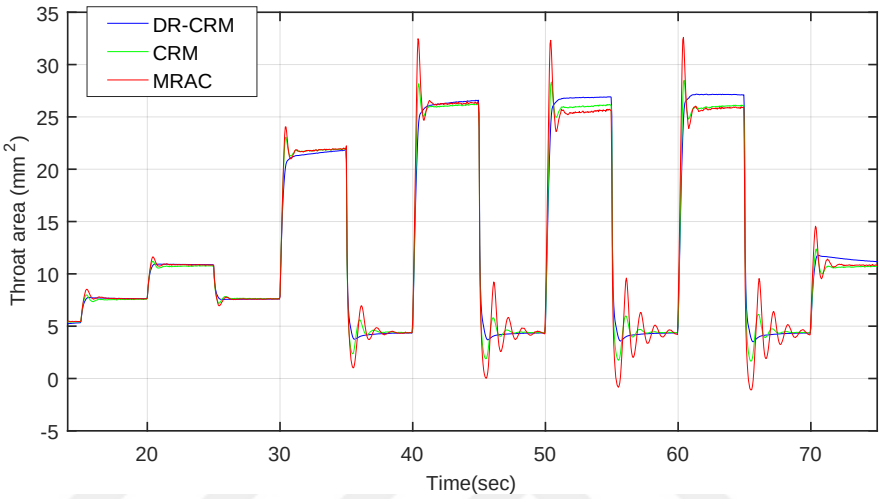

Figure 3.4: Evolution of control inputs of MRAC, CRM adaptive control and DR-CRM adaptive control in simulations.

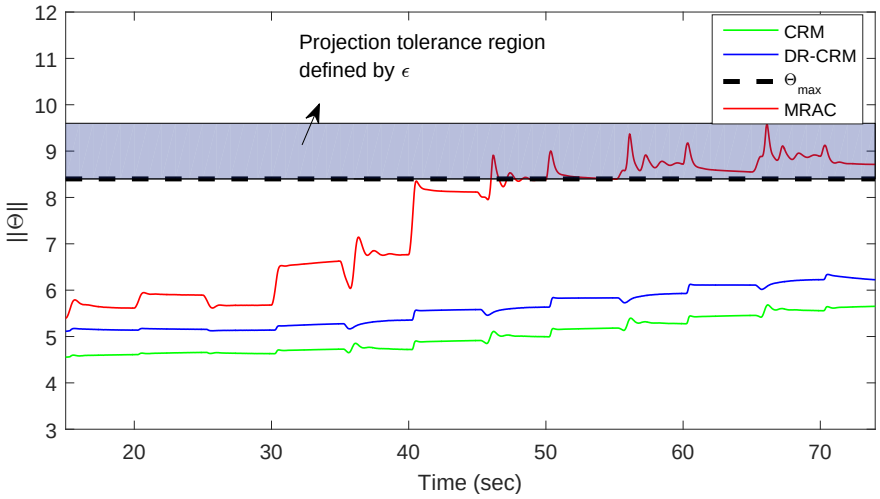

Figure 3.5: Controller parameters of MRAC, CRM adaptive control and DR-CRM adaptive control in simulations with the projection boundary

3.7.2 Gas Generator Simulations

In the gas generator control case, performance of MRAC is compared with the constant gain PI controller. In order to increase the simulation fidelity, burning time of the solid propellant is also included to the simulations by introducing a variable called "propellant mass" (see Table 3.3). As the propellant is burnt to generate fuel gas, its mass is decreased from the total mass using (2.3). When the propellant mass becomes finally zero, simulation halts, so that it gives a realistic image of the total operation time.

3.7.2.a MRAC vs. PI Controller

Tracking curves in the gas generator simulation for the PI controller and MRAC at three different operation points are given in Fig. 3.6. It can be observed from the simulation results that although the PI controller and MRAC show satisfactory performances around 50 bar operation pressure, PI controller presents an oscillatory response for higher pressure operating conditions and a slow response for lower pressures. On the other hand, MRAC can adapt itself to changing operating conditions and provides a more consistent performance across operating points.

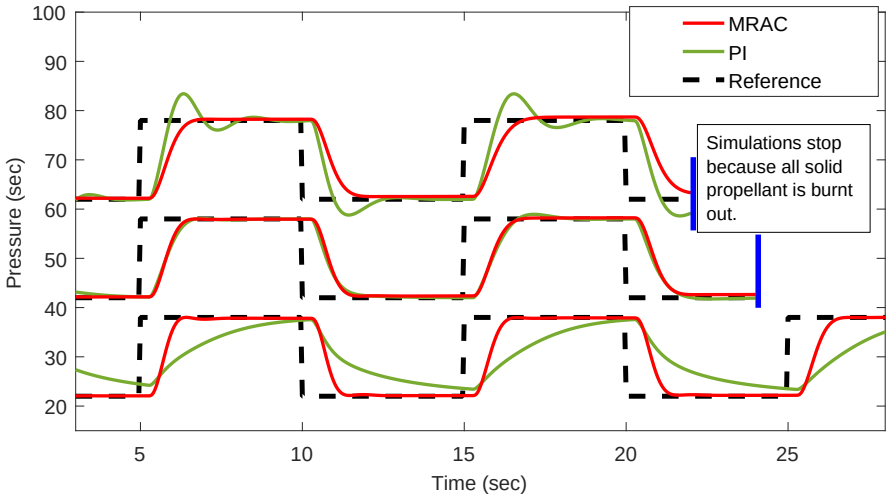

Figure 3.6: Tracking curves in gas generator simulation for the PI controller and MRAC at three different operating points. Simulation time at higher operating pressure is smaller compared to the operation at lower pressure since the solid propellant burns more rapidly.

Chapter 4

Experiments

The experimental results are obtained using a cold air test setup (CATS), which is provided by Roketsan Missiles Inc. (See Fig. 2.8 for a schematic of the overall system and Fig. 4.1 for the real experimental system). The pressure chamber in CATS has two ports, which are called the entrance port and the discharge port. The inlet port is connected to a nitrogen gas source of 230 bars through a pressure regulator. The pressure regulator ensures safe test conditions by adjusting the inflow pressure. There is a solenoid between the pressure chamber and the pressure regulator to stop the flow in case of emergencies. Outlet port of the pressure chamber has a shape of a nozzle whose effective throat area is continuously altered during the operation by the actuator and valve mechanism. An EC-max 30, 60 Watt, 24 Volt brushless direct current motor (Maxon Motor Company ®) with a EPOS2 70/10 driver is used as the actuator. Output shaft of the motor is connected to a gear box and a spindle, respectively. Other side of the spindle is connected to a conical pintle which is located such that its linear position determines the effective throat area at the outlet of the pressure chamber (see Fig. 2.9). There is a pressure transducer inside the pressure chamber, which provides real time pressure data to the controller. A slave Compact Rio computer (National Instrument ®), running LabVIEW software, is used to collect data from the pressure transducer, run the pressure controller cycles to calculate the necessary effective throat area and send this data to the actuator driver which

is responsible for controlling the actuator position.

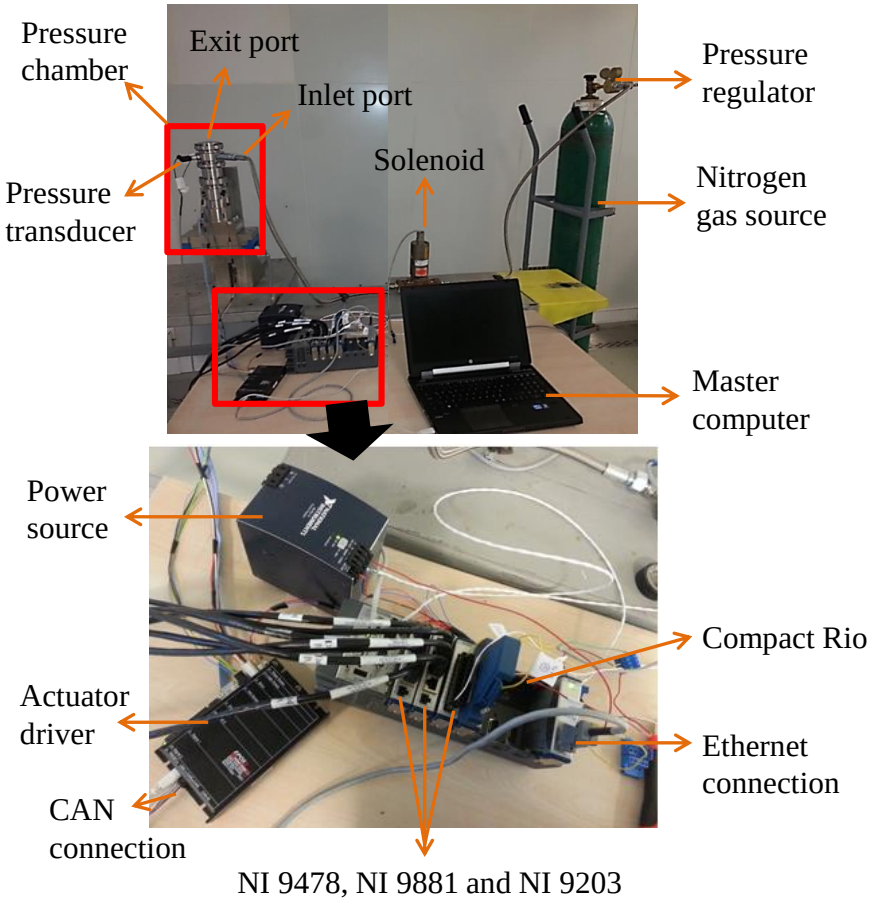

Figure 4.1: Cold air test setup.

The communication between the slave Compact Rio computer and the actuator driver card is through NI 9881 card using a CAN bus protocol. Pressure transducer is connected to the data acquisition card (NI 9203) that is also connected to the Compact Rio. All the algorithms for data acquisition, pressure controller calculations, data sending and corresponding communication phases are prepared in the master computer prior to the experiments using LabVIEW and the code is embedded to the slave Compact Rio computer through ethernet connection. Communication between the master and slave computers is realized with FIFO: First-In-First-Output methodology. Master computer monitors the experiment in real time and is able to intervene in the experimental process in case of a safety hazard. The solenoid located in between the pressure chamber

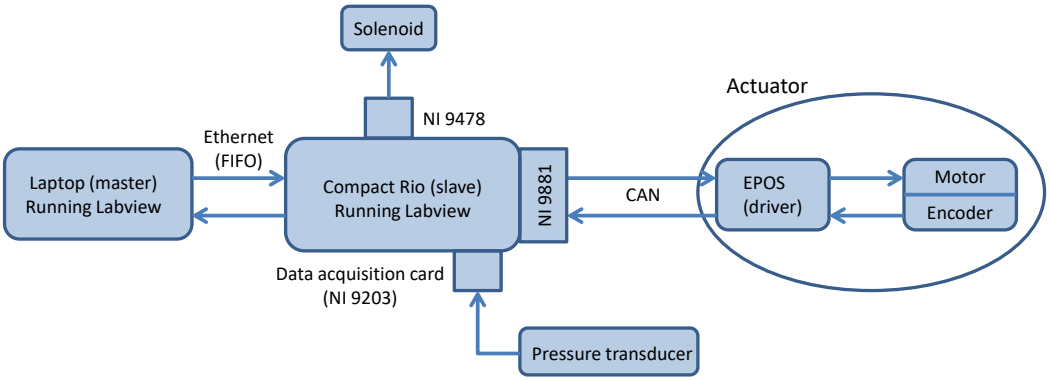

Figure 4.2: Schematic of the CATS hardware and data communication.

and the pressure regulator is controlled by the master computer through the digital card NI 9478. A detailed schematic of the hardware and data communication are given in Fig. 4.2.

The same scenarios used for the simulations are employed for the experimental tests. First, better performance of MRAC over the PI controller is demonstrated by performing experiments at three different operation points with the same controller gains and parameters used in the simulations. Then, a comparative evaluation showing the advantage of DR-CRM adaptive controller over other adaptive controllers are presented. Finally, an experiment is conducted for a larger period of time to show the effectiveness of the projection algorithm.

4.1 MRAC vs. PI Controller

Test results are given in Fig. 4.3. PI controller shows acceptable performance at the nominal operating point, the linearized model of which was used for the controller design. However, as the operating point deviates from the nominal design conditions, advantage of the adaptive controller, which provides consistent transient performance at different operating conditions, is observed.

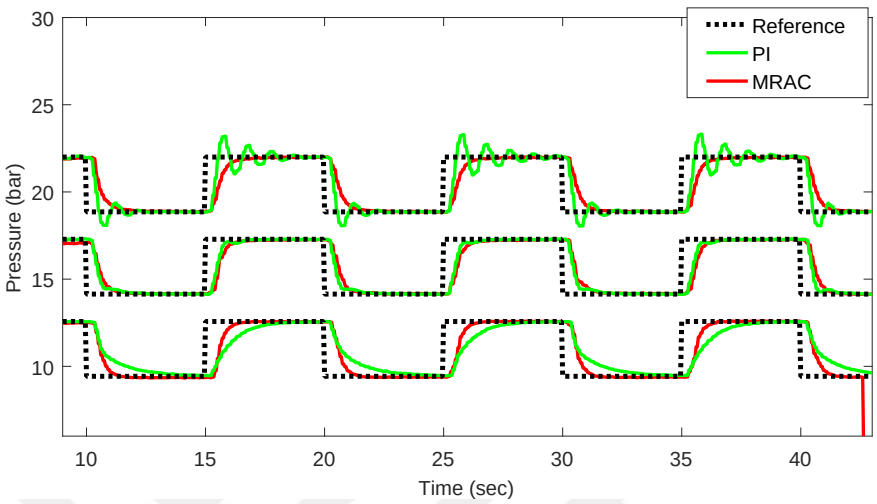

Figure 4.3: Test results of PI controller and MRAC for three different operating conditions. The adaptation rates used for these experiments are the same as the ones used in simulations.

4.2 Comparative Evaluation of Adaptive Controllers

To demonstrate the performance differences between the adaptive controllers, a more challenging reference signal, compared to that of the previous subsection, is used and time constant of the reference model, τ_m, is halved. Same controller design parameters are used as in the simulations.

Experiment results are given in Fig. 4.4-4.6, exhibiting similar trends with the simulations with CRM and DR-CRM adaptive controller having slightly more damped responses. DR-CRM adaptive controller is able handle the demanding operation conditions in the experiments and provides a reasonable performance. CRM adaptive controller, damping most of the oscillations as intended, results in undesired high amplitude overshoots. MRAC's response is similar to that of the other two adaptive controllers for small pressure deviation demands but becomes oscillatory for larger deviations in the reference signal. DR-CRM adaptive controller has the smoothest controller input, exhibited in Fig. 4.5. It is noted that the slight difference in the steady state values of the controller outputs is

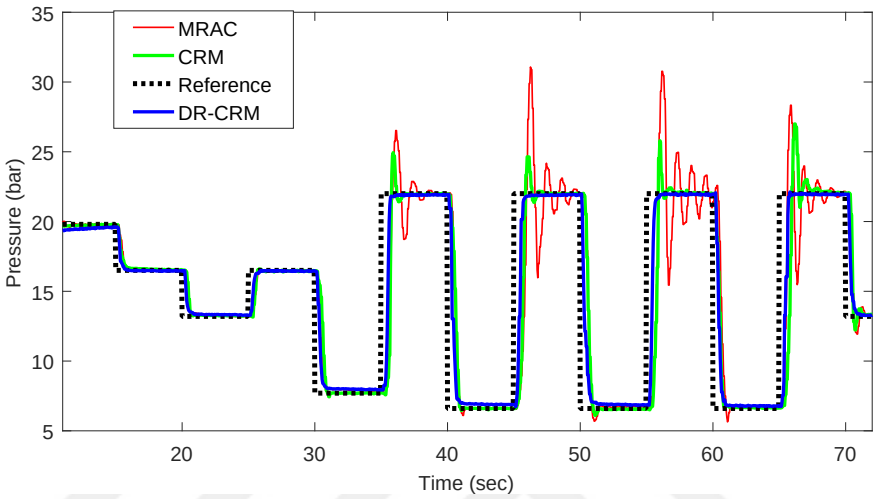

Figure 4.4: Reference tracking of MRAC, CRM adaptive control and DR-CRM adaptive control in experiments.

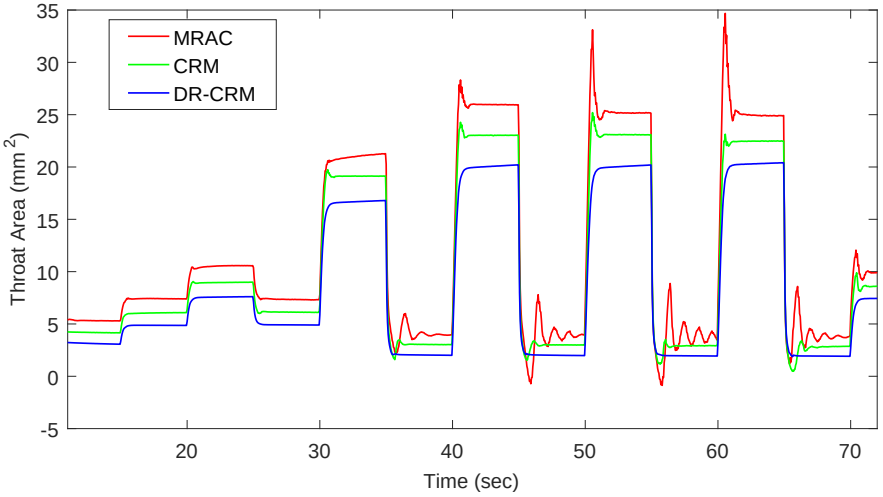

Figure 4.5: Evolution of control inputs of MRAC, CRM adaptive control and DR-CRM adaptive control in experiments.

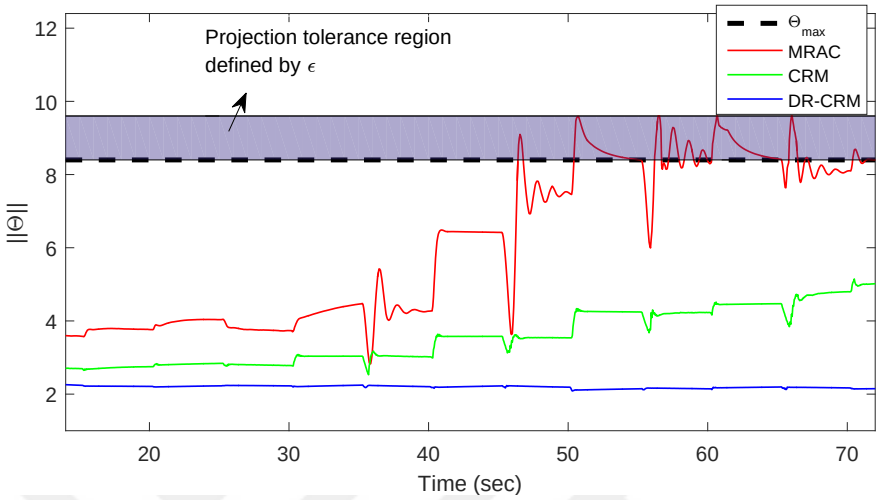

Figure 4.6: Controller parameters of MRAC, CRM adaptive control and DR-CRM adaptive control in experiments and projection boundary

due to the slightly different mass flow rate values of the experimental setup for different tests. Mass flow rate values reduce as more tests are conducted, which is considered to have insignificant affect on the experimental results. Fig. 4.6 shows that the controller parameters of MRAC hit the projection boundary, but then prevented to grow further.

Effect of the projection algorithm can be observed more clearly in the experiments that are conducted for longer times. Fig. 4.7 presents the evolution of the norm of the MRAC controller parameters in a longer test whose tracking curve is depicted in Fig. 4.8. Controller parameters tend to increase due to non-ideal situations such as unmodeled dynamics, disturbances and noise, but the projection algorithm keeps them within a predefined bound.

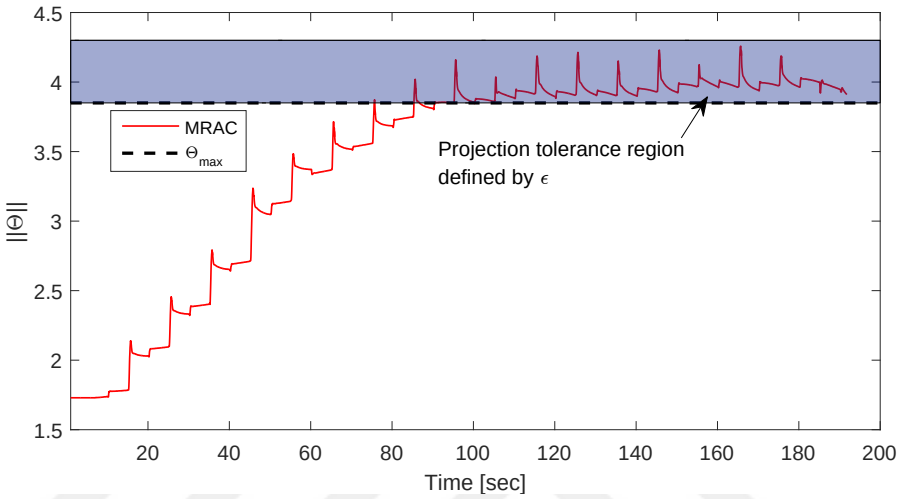

Figure 4.7: Controller parameters in the long-term test

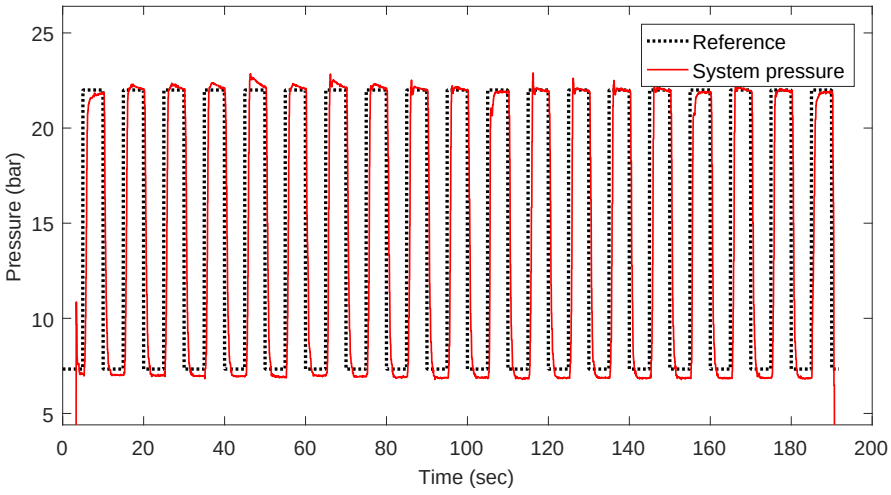

Figure 4.8: Pressure tracking in the long-term test

Chapter 5

Conclusion and Future Work

Having variable thrust during the operation for a rocket provides a tremendous advantage while chasing down a target. For ducted rockets, the key factor to obtain variable thrust is the precise pressure control of the gas generator, which is addressed in this thesis. To solve this control problem, which includes time delays, uncertainties and nonlinear dynamics, a delay resistant closed loop reference model (DR-CRM) adaptive controller is proposed. The controller merges the benefits of two different approaches: The first approach is the adaptive posicast controller (APC) which compensates the time delay by making use of positively forecasted output of the plant. The second approach is the closed-loop reference model (CRM) modification, which damps the high frequency oscillations due to high adaptive learning rates by altering the reference model structure with tracking error feedback. DR-CRM adaptive controller is tested using a cold air test setup which is utilized as a test bed for throttleable ducted rocket development.

To address the control problem, first, mathematical model of the gas generator (GG) system is derived for all elements in detail. Besides the GG, the model of the cold air testing setup (CATS) is also determined and employed, together with the real experimental system, to have a comparative evaluation between the designed controllers. In order to facilitate the controller design, models are simplified using linearization and ignoring the fast actuator dynamics. Furthermore,

nonlinear model of CATS is improved to have a high fidelity model in simulations by updating parameters using open loop experiments.

The controllers need to be robust enough against the uncertainties and disturbances in the plant emanating from the ablation and deposition at the throat, modeling inaccuracies and model simplifications. Time delays are also observed in the experimental setup, which makes the control problem even more challenging. In order to address these challenges, four different controllers are designed: Model reference adaptive controller (MRAC), closed loop reference model (CRM) adaptive controller, the delay resistant closed loop reference model (DR-CRM) adaptive controller and a proportional-integral (PI) controller. Adaptive controllers are enforced with a robustfying modification called as the projection algorithm, which is utilized to ensure the boundedness of the controller parameters. A step-by-step procedure of adaptive controller design is also included to help the design and the implementation process easier.

Performances of all controllers are first evaluated in simulations utilizing full nonlinear models. MRAC clearly demonstrates its advantage over constant gain PI controller. More demanding conditions, such as larger deviations in the desired pressures, reveal the advantage of DR-CRM adaptive controller over CRM adaptive controller and MRAC. The effect of the projection algorithm to ensure the boundedness of the controller parameters are also shown in the simulations. All four controllers' performances are compared experimentally in CATS. Similar conclusions with the simulations are drawn. Adaptive controllers reveal their superiority over the PI controller by adapting to changing operating points and conditions. DR-CRM adaptive controller demonstrates improved results compared to the other adaptive controllers when the desired pressure variations from the closed loop system is increased.

The results of this research show that combining different control approaches is effective in addressing complex control problems such as gas generator pressure control.

The proposed adaptive controller, DR-CRM, is ready for the implementation

on a real gas generator, which is left as a future work. The study on improving/modifying the proposed approach is expected to continue based on the new requirements originating from the gas generator implementation requirements. These requirements may arise due to time-varying or uncertain time delays, the need for discrete domain design due to non-ideal sampling or different kind of disturbances that require more sophisticated disturbance rejection methods.

Bibliography

[1] W. Miller, S. McClendon, and W. Burkes, "Design approaches for variable flow ducted rockets," in *Proc. AIAA/SAE/ASME 17th Joint Propulsion Conference*, (Colorado Springs, Colorado), 1981.

[2] C. Goldman and A. Gany, "Thrust modulation of ram-rockets by a vortex valve," in *AIAA, ASME, SAE, and ASEE, Joint Propulsion Conference and Exhibit*, (Lake Buena Vista, FL), 1996.

[3] H.-L. Besser and G. Kurth, "Meteor - european air dominance missile powered by high energy throttleable ducted rocket," in *Proc. RTO-MP-AVT-208*, pp. 1–17, 2012.

[4] S. Burroughs, "Status of army pintle technology for controllable thrust propulsion," in *37th AIAA/ASME/SAE/ASEE Joint Propulsion Conference and Exhibit*, (Salt Lake City, Utah), 2001.

[5] K. Xie, Y. Liu, L. Qin, X. Chen, Z. Lin, and S. Liang, "Experimental and numerical studies on combustion character of solid-liquid rocket ramjet," in *45th AIAA/ASME/SAE/ASEE Joint Propulsion Conference*, no. AIAA-2009-5124, (Denver, Colorado), 2009.

[6] C. Bauer, F. Davenne, N. Hopfe, and G. Kurthy, "Modeling of a throttleable ducted rocket propulsion system," in *Proc. AIAA/ASME/ASEE Joint Propulsion Conference & Exhibit*, (San Diego, California), pp. 1–15, 2011.

[7] C. Bauer, N. Hopfe, P. Caldas-Pinto, F. Davenne, and G. Kurth, "Advanced flight performance evaluation methods of supersonic air- breathing propulsion system by a highly integrated model based approach," in *Proc. RTO-MP-AVT-208*, pp. 1–14, 2012.

[8] A. Atwood, T. Boggs, T. P. P.O. Curran, and D. Hanson-Parr, "Burning rate of solid propellant ingredients, part 1: Pressure and initial temperature effects," *Journal of Propulsion and Power*, vol. 15, pp. 740–747, November-December 1999.

[9] J. Chang, B. Li, W. Bao, W. Niu, and D. Yu, "Thrust control system design of ducted rockets," *Acta Astronautica*, vol. 69, no. 1, pp. 86–95, 2011.

[10] W. Bao, B. Li, J. Chang, W. Niu, and D. Yu, "Switching control of thrust regulation and inlet buzz protection for ducted rocket," *Acta Astronautica*, vol. 67, no. 7, pp. 764–773, 2010.

[11] W. Bao, Y. Qi, and J. Chang, "Multi-objective regulating and protecting control for ducted rocket using a bumpless transfer scheme," *Proceedings of the IMechE, Part G:Journal of Aerospace Engineering*, pp. 311–325, 2012.

[12] Y. Qi, W. Bao, J. Zhao, and J. Chang, "Coordinated control for regulation/protection mode-switching of ducted rockets," *Acta Astronautica*, vol. 98, pp. 138–146, 2014.

[13] W. Bao, W. Niu, C. J.T., T. Cui, and D. Yu, "Control system design and experiment of needle-type gas regulating system for ducted rocket," *Proceedings of the Institution of Mechanical Engineers, Part G, Journal of Aerospace Engineering*, vol. 224, no. 5, pp. 563–573, 2010.

[14] Y. Qi, W. Bao, J. Chang, and J. Cui, "Fast limit protection design: A terminal sliding mode control method," in *Proceedings of the 33rd Chinese Control Conference*, (Nanjing, China), 2014.

[15] M. Ostrander and M. Thomas, "Air turbo-rocket solid propellant development and testing," in *Proc. AIAA/ASME/SAE/ASEE 33th Joint Propulsion Conference and Exhibit*, 1997.

[16] J. L. Bergmans and R. D. Salvo, "Solid rocket motor control: theoretical motivation and experimental demonstration," in *Proc. AIAA/ASME/SAE/ASEE 39th Joint Propulsion Conference and Exhibit*, pp. 20–23, 2003.

[17] D. Thomaier, "Speed control of a missile with throttleable ducted rocket propulsion," in *Proc. Advances in Air-Launched Weapon Guidance and Control 15 p (SEE N88-19553 12-15)*, 1987.

[18] A. G. Sreeriatha and N. Bhardwaj, "Mach number control-ler for a flight vehicle with ramjet propulsion," in *Proc. AIAA/ASME/SAE/ASEE 35th Joint Propulsion Conference and Exhibit*, no. AIAA 99-294, (Los Angeles, CA), 1999.

[19] P. Pinto and G. Kurth, "Robust propulsion control in all flight stages of a throtteable ducted rocket," in *Proc. AIAA/ASME/ASEE Joint Propulsion Conference & Exhibit*, no. AIAA-2011-5611, (San Diego, California), pp. 1–12, 2011.

[20] S. Joner and I. Quinquis, "Control of an exoatmospheric kill vehicle with a solid propulsion attitude control system," in *AIAA Guidance, Navigation, and Control Conference and Exhibit*, no. AIAA 2006-6572, (Keystone, Colorado), 2006.

[21] A. Ilchmann, E. P. Ryan, and C. J. Sangwin, "Tracking with prescribed transient behaviour," *ESAIM: Control, Optimisation and Calculus of Variations*, vol. 7, pp. 471–493, 2002.

[22] J. L. Bergmans and R. I. Myers, "Throttle valves for air tur-bo-rocket engine control," in *Proc. AIAA/ASME/SAE/ASEE 33th Joint Propulsion Conference and Exhibit*, 1997.

[23] Z. W. Peterson, S. D. Eilers, and S. A. Whitmorey, "Closed-loop thrust and pressure profile throttling of a nitrous-oxide htpb hybrid rocket motor," in *48th AIAA/ASME/SAE/ASEE Joint Propulsion Conference and Exhibit*, (Atlanta, Georgia), 2012.

[24] C. A. Davis and A. B. Gerards, "Variable thrust solid propulsion control using labview," in *Proc. AIAA/ASME/SAE/ASEE 39th Joint Propulsion Conference and Exhibit*, no. AIAA 2003-5241, (Huntsville, Alabama), 2003.

[25] Y. Yildiz, A. Annaswamy, I. Kolmanovsky, and D. Yanakiev, "Adaptive posicast controller for time-delay systems with relative degree $n^* \leq 2$," *Automatica*, vol. 46, no. 2, pp. 279–289, 2010.

[26] T.Gibson, A.Annaswamy, and E.Lavretsky, "Adaptive systems with closed-loop reference models: Stability, robustness, and transient performance," *arXiv:1201.4897. Ithaca, NY: Cornell University Library. Retrieved from http://arxiv.org/abs/1201.4897.*

[27] T.Gibson, A.Annaswamy, and E.Lavretsky, "Improved transient response in adaptive control using projection algorithms and closed loop reference models," in *AIAA Guidance, Navigation, and Control Conference*, no. AIAA-2012-4775, (Minneapolis, Minnesota), 2012.

[28] T.Gibson, A.Annaswamy, and E.Lavretsky, "On adaptive control with closed-loop reference models: Transients, oscillations, and peaking," *IEEE Access*, vol. 1, pp. 709–717, Sept. 2013.

[29] O. J. Smith, "A controller to overcome dead time," *ISA Journal*, vol. 6, 1959.

[30] A. Z. Manitius and A. W. Olbrot, "Finite spectrum assignement problem for systems with delays," *IEEE Transactions on Automatic Control*, vol. 24, no. 4, 1979.

[31] K. Ichikawa, "Frequency-domain pole assignement and exact model-matching for delay systems," *International Journal of Control*, vol. 41, pp. 1015–1024, 1985.

[32] R. Ortega and R. Lozano, "Globally stable adaptive controller for systems with delay," *International Journal of Control*, vol. 47, no. 1, pp. 17–23, 1988.

[33] S.-I. Niculescu and A. M. Annaswamy, "An adaptive smith-controller for time-delay systems with relative degree $n^* \leq 2$," *Systems and Control Letters*, vol. 49, pp. 347–358, 2003.

[34] Y. Yildiz, A. Annaswamy, D. Yanakiev, and I. Kolmanovsky, "Spark ignition engine idle speed control: An adaptive control approach," *IEEE Transactions On Control Systems Technology*, vol. 19, no. 5, pp. 990–1002, 2011.

[35] Y. Yildiz, A. Annaswamy, D. Yanakiev, and I. Kolmanovsky, "Spark ignition engine fuel-to-air ratio control: An adaptive control approach," *Control Engineering Practice*, vol. 18, no. 12, pp. 1369–1378, 2010.

[36] Y. Yildiz, A. Annaswamy, D. Yanakiev, and I. Kolmanovsky, "Adaptive idle speed control for internal combustion engines," in *Proc. Amer. Control Conf.*, (New York City), pp. 3700–3705, July 2007.

[37] Y. Yildiz, A. Annaswamy, D. Yanakiev, and I. Kolmanovsky, "Automotive powertrain control problems involving time delay: An adaptive control approach," in *Proc. ASME Dynamic Systems and Control Conference*, (Ann Arbor, Michigan), Oct. 2008.

[38] Y. Yildiz, A. Annaswamy, D. Yanakiev, and I. Kolmanovsky, "Adaptive air fuel ratio control for internal combustion engines," in *Proc. Amer. Control Conf.*, (Seattle, Washington), pp. 2058–2063, June 2008.

[39] Z.T.Dydek, A.Annaswamy, J.J.E.Slotine, and E.Lavretsky, "Composite adaptive posicast control for a class of lti plants with known delay," *Automatica*, vol. 49, pp. 1914–1924, March 2013.

[40] D. Bresch-Pietri and M. Krstic, "Adaptive trajectory tracking despite unknown input delay and plant parameters," *Automatica*, vol. 45, pp. 2074–2081, September 2009.

[41] N. Bekiaris-Liberis and M. Krstic, "Delay-adaptive feedback for linear feedforward systems," *System and Control Letters*, vol. 59, pp. 277–283, May 2010.

[42] M. Krstic, *Delay Compensation for Nonlinear, Adaptive, and PDE Systems*. Boston: Birkhauser, 2009.

[43] T.Gibson, A.Annaswamy, and E.Lavretsky, "Closed-loop reference models for output-feedback adaptive systems," in *European Control Conference (ECC)*, (IEEE, Zurich), pp. 365–370, 2013.

[44] T.Gibson, A.Annaswamy, and E.Lavretsky, "Adaptive systems with closed-loop reference models, part i: Transient performance," in *American Control Conference*, (IEEE, Piscataway, NJ), pp. 3376–3383, 2013.

[45] E. Lavretsky, "Adaptive output feedback design using asymptotic properties of lqg/ltr controllers," *IEEE Trans. Automat. Contr.*, vol. 57, no. 6, 2012.

[46] V. Stepanyan and K. Krishnakumar, "Mrac revisited: guaranteed perforamance with reference model modification," in *American Control Conference*, 2010.

[47] V. Stepanyan and K. Krishnakumar, "Mmrac for nonlinear systems with bounded disturbances," in *Conference on Decision and Control*, 2011.

[48] T. Yucelen, G. D. L. Torre, and E. N. Johnson, "Improving transient performance of adaptive control architectures using frequency-limited system error dynamics," *International Journal of Control*, vol. DOI:10.1080/00207179.2014.922702, 2014.

[49] J. H. Lee, B. H. Park, and W. Yoon, "Parametric investigation of the pintle-perturbed conical nozzle flows," *Aerospace Science and Technology*, vol. 26, no. 5, pp. 268–279, 2013.

[50] R. Deng, T. Setoguchi, and H. D. Kim, "Computational study on the thrust performance of a supersonic pintle nozzle," in *International Symposium of Turbulence and Shear Flow Phenomena*, (Melbourne, Australia), 2015.

[51] J. Heo, K. Jeong, and H.-G. Sung, "Numerical study of the dynamic characteristics of pintle nozzles for variable thrust," *JOURNAL OF PROPULSION AND POWER*, vol. 31, no. 1, pp. 230–237, 2015.

[52] H. Ko, J.-H. Lee, H.-B. Chang, and W.-S. Yoon, "Cold tests and the dynamic characteristics of the pintle type solid rocket motor," in *49th*

AIAA/ASME/SAE/ASEE Joint Propulsion Conference, (San Jose, CA), 2013.

[53] J. H. Lee, J. K. Kim, H. B. Jang, and J. Y. Oh, "Experimental and theoretical investigations of thrust variation with pintle positions using cold gas," in *44th AIAA/ASME/SAE/ASEE Joint Propulsion Conference and Exhibit*, (Hartford, CT), 2008.

[54] S. B. Verma and O. Haidn, "Cold gas testing of thrust-optimized parabolic nozzle in a high-altitude test facility," *Journal of Propulsion and Power*, vol. 27, pp. 1238–1246, November-December 2011.

[55] W. Y. Niu, W. Bao, J. Chang, T. Cui, , and D. R. Yu, "Control system design and experiment of needle-type gas regulating system for ducted rocket," *Journal of Aerospace Engineering*, vol. 224, no. 5, pp. 563–573, 2010.

[56] H. SHEKHAR, "Mathematical formulation and validation of muraours linear burning rate law for solid rocket propellants," *Central European Journal of Energetic Materials*, vol. 9, no. 4, pp. 353–364, 2012.

[57] K. S. Narendra and A. M. Annaswamy, *Stable adaptive systems*. New York: Dover Publications, 2005.

[58] E. Lavretsky and K. A. Wise, *Robust Adaptive Control*. London: Springer, 2013.

[59] Y. Yildiz, A. M. Annaswamy, D. Yanakiev, and I. Kolmanovsky, "Spark-ignition-engine idle speed control: An adaptive control approach," *IEEE TRANSACTIONS ON CONTROL SYSTEMS TECHNOLOGY*, vol. 19, pp. 990–1002, September 2011.

[60] T. E. Gibson, *Closed-Loop Reference Model Adaptive Control: with Application to Very Flexible Aircraft*. Phd thesis, Massachusetts Institute of Technology, 2014.

Appendix A

Memory Requirement and Computational Load of the Implementation of the DR-CRM Adaptive Controller

Input time delay is observed to be 300 ms on the average, whereas sampling interval of the controller cycle is chosen as 50 ms, which adds 6 controller parameters, λ_i, and 6 states, $u(t - mdt)$, to the controller structure (see (3.50)). There are 9 states overall, 9 controller parameters, 9 multiplication results, which adds up to 1 controller signal. We need 9 terms to the define adaptation laws, 4 terms to define reference model (a_m, b_m, ℓ and y_m), 1 tracking error term and 9 adaptation rate terms. In addition, we need 13 terms for the projection algorithm ($\Theta_{max}, \epsilon, ||\Theta||, f$ and ∇f). Overall, we have 64 float variables that needs 256 bytes of memory space.

9 multiplication and 8 summation operations are needed to define the controller signal. There exist 18 multiplications in the adaptive law calculations and 9 summation operations are required to update the controller parameters. In addition, 4 summation and 3 multiplication operations are needed to be employed

to form the reference model output and the tracking error. Furthermore, in the projection algorithm, there are 2 comparison and 1 logical operations, 18 summation and 43 multiplication operations along with a square root operator. In total, 116 floating point operations are conducted per controller cycle that runs with a sampling rate of 50 ms, which results in 2320 floating point operations per second (FLOPS).